

1 **Early season mesopelagic carbon remineralization and transfer**  
2 **efficiency in the naturally iron-fertilized Kerguelen area**

3

4 Jacquet S.H.M.<sup>1</sup>, F. Dehairs<sup>2</sup>, D. Lefèvre<sup>1</sup>, A.J. Cavagna<sup>2</sup>, F. Planchon<sup>3</sup>,  
5 U. Christaki<sup>4</sup>, L. Monin<sup>5</sup>, L. André<sup>5</sup>, I. Closset<sup>6</sup> and D. Cardinal<sup>6</sup>

6

7 <sup>1</sup>Aix Marseille Université, CNRS/INSU, IRD, Mediterranean Institute of  
8 Oceanography (MIO), UM 110, 13288 Marseille, France

9

10 <sup>2</sup>Vrije Universiteit Brussel, Analytical, Environmental & Geo-Chemistry  
11 and Earth System Sciences, Brussels, Belgium

12

13 <sup>3</sup>Laboratoire des Sciences de l'Environnement Marin (LEMAR),  
14 Université de Brest, CNRS, IRD, UMR 6539, IUEM; Technopôle Brest  
15 Iroise, Place Nicolas Copernic, F-29280 Plouzané, France

16

17 <sup>4</sup>INSU-CNRS, UMR8187 LOG, Laboratoire d'Océanologie et de  
18 Géosciences, Université du Littoral Côte d'Opale, ULCO, 32 avenue  
19 Foch, 62930 Wimereux, France

20

21 <sup>5</sup>Earth Sciences Department, Royal Museum for Central Africa,  
22 Leuvensesteenweg 13, Tervuren, B 3080, Belgium

23

24 <sup>6</sup>Sorbonne Universités (UPMC, Univ Paris 06)-CNRS-IRD-MNHN,  
25 LOCEAN Laboratory, 4 place Jussieu, F-75005 Paris, France

26

27 **Corresponding author:** [stephanie.jacquet@mio.osupytheas.fr](mailto:stephanie.jacquet@mio.osupytheas.fr)

28

29 **Abstract**

30 We report on the zonal variability of mesopelagic particulate organic carbon  
31 remineralization and deep carbon transfer potential during the Kerguelen  
32 Ocean and Plateau compared Study 2 expedition (KEOPS 2; Oct.-Nov. 2011)  
33 in an area of the Polar Front supporting recurrent massive blooms from  
34 natural Fe fertilization. Mesopelagic carbon remineralization (MR) was  
35 assessed using the excess, non-lithogenic particulate barium ( $Ba_{xs}$ )  
36 inventories in mesopelagic waters and compared with bacterial production  
37 (BP), surface primary production (PP) and export production (EP). Results for  
38 this early season study are compared with results obtained during a previous  
39 study (2005; KEOPS 1) for the same area at a later stage of the  
40 phytoplankton bloom. Our results reveal the patchiness of the season  
41 advancement and of the establishment of remineralization processes between  
42 plateau (A3) and Polar Front sites during KEOPS 2. For the Kerguelen plateau  
43 (A3 site) we observe a similar functioning of the mesopelagic ecosystem  
44 during both seasons (spring and summer), with low and rather stable  
45 remineralization fluxes in the mesopelagic column (150-400 m). The shallow  
46 water column ( $\sim 500$ m), the lateral advection, the zooplankton grazing  
47 pressure and the pulsed nature of the POC transfer at A3 seem to drive the  
48 extend of MR processes on the plateau. For deeper stations ( $>2000$  m)  
49 located on the margin, inside a Polar Front meander, as well as in the vicinity  
50 of the Polar Front, east of Kerguelen, remineralization in the upper 400 m in  
51 general represents a larger part of surface carbon export, but when  
52 considering the upper 800 m, in some cases, the entire flux of exported  
53 carbon is remineralized. In the Polar Front meander, where successive  
54 stations form a time series, two successive events of particle transfer were  
55 evidenced by remineralization rates: a first mesopelagic and deep transfer  
56 from a past bloom before the cruise, and a second transfer expanding at  
57 mesopelagic layers during the cruise. Regarding the deep carbon transfer

58 efficiency, it appeared that above the plateau (A3 site) the mesopelagic  
59 remineralization was not a major barrier to the transfer of organic matter to  
60 the sea-floor (close to 500 m). There the efficiency of carbon transfer to the  
61 bottom waters (>400 m) as assessed by PP, EP and MR fluxes comparisons  
62 reached up to 87% of the carbon exported from the upper 150 m. In contrast,  
63 at the deeper locations mesopelagic remineralization clearly limited the  
64 transfer of carbon to depths >400 m. For sites at the margin of the plateau  
65 (station E-4W) and the Polar front (station F-L), mesopelagic remineralization  
66 even exceeded upper 150 m export, resulting in a null transfer efficiency to  
67 depths >800 m. In the Polar Front meander (time series), the capacity of the  
68 meander to transfer carbon to depth >800 m was highly variable (0 to 73 %).  
69 The highest carbon transfer efficiencies in the meander are furthermore  
70 coupled to intense and complete deep (>800 m) remineralization, resulting  
71 again in a close to zero deep (>2000 m) carbon sequestration efficiency  
72 there.

73

74 Key Words: particulate barium, mesopelagic carbon remineralization, carbon  
75 transfer efficiency, Southern Ocean

76

77 **1. INTRODUCTION**

78 While numerous artificial (Boyd et al., 2000, 2004; Gervais et al.,  
79 2002; Buesseler et al., 2004, 2005; de Baar et al., 2005; Hoffmann et al.,  
80 2006; Boyd et al., 2012; Smetacek et al., 2012) and natural (Blain et al.,  
81 2007; Pollard et al., 2009; Zhou et al., 2010, 2013) ocean iron-fertilization  
82 experiments in the Southern Ocean demonstrated the role of iron in  
83 enhancing the phytoplankton biomass and production in high-nutrient low-  
84 chlorophyll (HNLC) regions, determining to what extent fertilization could  
85 modify the transfer of particulate organic carbon (POC) to the deep ocean is  
86 far from being comprehensively achieved (Lampitt et al., 2008; Morris and  
87 Charette, 2013; Le Moigne et al., 2014; Robinson et al., 2014). This is partly  
88 due to the short term over which the observations were made, precluding  
89 extrapolation to longer time scales. Moreover, when assessing whether Fe-  
90 supply could induce vertical POC transfer, the magnitude of the export from  
91 surface is not the only important parameter to take into account. Indeed, POC  
92 fate in the mesopelagic zone (defined as 100-1000 m depth layer) is often  
93 largely overlooked although these depth layers are responsible for the  
94 remineralization of most of the POC exported from the surface layer (Martin et  
95 al., 1987; Longhurst, 1990; Lampitt and Antia, 1997; François et al., 2002;  
96 Buesseler et al., 2007b; Buesseler and Boyd, 2009). Only few studies  
97 considered mesopelagic carbon (C) remineralization rates (Buesseler et al.,  
98 2007a; Jacquet et al., 2008a, 2008b, 2011a, 2011b; Salter et al., 2007) to  
99 estimate the response of deep POC export to fertilization. Assessing  
100 mesopelagic C remineralization is pivotal to evaluate remineralization length  
101 scale as well as the time scale of the C storage in the deep ocean. Indeed the  
102 typical depth of the main thermocline, 1000 m (IPCC, WG1, 2007, chp5) is  
103 often referred to as the horizon clearly removed from the surface ocean and  
104 atmosphere (Passow and Carlson, 2012). Overall, assessing mesopelagic C  
105 remineralization will allow to better quantify the ocean's biological carbon

106 pump and its efficiency in the global C cycle which bears large uncertainty and  
107 is currently under debate (e.g. from 5 Gt/yr in [Henson et al., 2011](#) to 21 Gt  
108 C/yr in [Laws et al., 2000](#) and 13 Gt/yr in [IPPC WG1 report \(ch. 6, 2013\)](#)).

109 The present work aims at understanding the impact of a natural iron-  
110 induced bloom on the mesopelagic POC remineralization and zonal variability  
111 in the Kerguelen area (Southern Ocean). Here, C remineralization was  
112 assessed from particulate biogenic Ba (hereafter called excess-Ba or  $Ba_{xs}$ ;  
113 mainly forms as barite  $BaSO_4$  crystals) contents in the mesopelagic water  
114 column. The link between barite and C remineralization resides in the fact that  
115 this mineral precipitates inside oversaturated micro-environments (biogenic  
116 aggregates) during the process of prokaryotic degradation of sinking POC  
117 ([Dehairs et al., 1980, 1992, 1997, 2008](#); [Stroobants et al., 1991, Cardinal et](#)  
118 [al., 2001, 2005](#); [Jacquet et al., 2007, 2008b, 2011a](#); [Planchon et al., 2013](#);  
119 [Sternberg et al. 2007, 2008a, 2008b](#)). Once the aggregates have been  
120 remineralized, barites are released and spread over the mesopelagic layer.  
121 Overall, earlier work highlights the fact that suspended barite in mesopelagic  
122 waters builds up over the growing season and reflects past remineralization  
123 activity integrated over several days to weeks ([Dehairs et al., 1997](#); [Cardinal](#)  
124 [et al., 2005](#); [Jacquet et al., 2007, 2008b](#)). An algorithm relating mesopelagic  
125  $Ba_{xs}$  contents to oxygen consumption ([Shopova et al., 1995](#); [Dehairs et al.,](#)  
126 [1997](#)) allowed remineralization of POC fluxes to be estimated for the  
127 mesopelagic layer. Combined with surface C production and export estimates,  
128 mesopelagic  $Ba_{xs}$  also informs on the efficiency of the system toward deep  
129 carbon transfer. From earlier studies, the efficiency of C transfer through the  
130 mesopelagic layer was reported to increase under artificially induced (EIFEX;  
131 [Strass et al., 2005](#); [Smetacek et al., 2012](#)) and natural (KEOPS; [Blain et al.,](#)  
132 [2007](#)) Fe-replete conditions ([Jacquet et al., 2008a, 2008b](#); [Savoie et al.,](#)  
133 [2008](#)) compared to Fe-limited, non-bloom, HNLC reference stations in the  
134 Southern Ocean. In contrast, C transfer efficiency through the mesopelagic

135 layer was reported smaller in natural Fe-replete locations during the SAZ-  
136 Sense cruise off Tasmania (Jacquet et al., 2011a, 2011b). Differences in  
137 plankton community structure and composition (e.g. diatoms vs. flagellates,  
138 type of diatoms) were pointed at, as possible causes of such discrepancies in  
139 C transfer efficiency through the mesopelagic layer (Jacquet et al., 2008a,  
140 2011a, 2011b). Also, differences in integration time scales for the processes  
141 that control the carbon fluxes in artificially vs. naturally Fe fertilized systems,  
142 may yield an incomplete picture of the C transfer potential and lead to  
143 misleading conclusions.

144 Here, we examine changes in mesopelagic POC remineralization  
145 during the early spring (Oct. –Nov. 2011) KEOPS 2 expedition to the naturally  
146 iron fertilized area eastward of Kerguelen Islands. The hydrographic structure  
147 of the Kerguelen area generates contrasted environments that are differently  
148 impacted by iron availability and mesoscale activity. The specific objectives of  
149 the present work are to assess the zonal variability of mesopelagic C  
150 remineralization and deep C transfer potential, and to identify possible causes  
151 inducing this variability. As the same area was visited earlier in 2005 during  
152 summer at a late stage of the bloom (KEOPS 1; Jan.-Feb., 2005), this  
153 condition offers a unique opportunity to estimate the main carbon fluxes over  
154 most of the growth season. Mesopelagic C remineralization estimates are  
155 compared to particle and biological parameters as reported in other papers  
156 included in this issue (Cavagna et al., 2014; Christaki et al., 2014; Dehairs et  
157 al., 2014; Lasbleiz et al., 2014; Laurenceau-Cornec et al., 2015; Planchon et  
158 al., 2014; van der Merve et al., 2015) and in Blain et al., (2007), Christaki et  
159 al. (2008), Jacquet et al., (2008a), Park et al., (2008) and Savoye et al.,  
160 (2008).

161

## 162 **2. EXPERIMENT AND METHODS**

### 163 **2.1. Study area**

164           The KEOPS 2 (Kerguelen Ocean and Plateau compared Study) cruise  
165 was conducted in austral spring at the onset of the bloom from 10 October to  
166 20 November aboard the R/V *Marion Dufresne* (TAAF/IPEV). The KEOPS 2  
167 expedition studied the Kerguelen Plateau area (Indian sector of the Southern  
168 Ocean) which is characterized by the passage of the Polar Front (PF), as  
169 illustrated in Fig.1a. The Kerguelen Plateau is surrounded by the Antarctic  
170 Circumpolar Current (ACC) whose main branch circulates to the north of the  
171 plateau (Park et al., 2008). A second branch of the ACC circulates to the  
172 south of Kerguelen Islands to further join a branch of the Fawn Trough  
173 Current (FTC). The FTC has a main northeast direction, but a minor branch  
174 splits away northwestward to join the eastern side of the Kerguelen plateau  
175 (Park et al., 2008; Fig1.a). These particular hydrographic features generate a  
176 mosaic of recurrent massive bloom patterns in the northeastern part of the  
177 Plateau and the possible sources and mechanisms for fertilization were  
178 investigated during ANTARES 3 (1995; Blain et al., 2001) and KEOPS 1 cruise,  
179 later referred to as KEOPS 1 (Jan.-Feb. 2005, late summer conditions; Blain  
180 et al., 2007, 2008). During KEOPS 2 the evolution of Chl-a data based on  
181 multi-satellite imagery of the study area revealed the presence of different  
182 Chl-a rich plumes (D’ovidio et al., 2015) (Fig.1a; e.g. Chl-a map from  
183 11/11/2011). Stations were sampled in distinct zones covering these different  
184 bloom patterns (Fig.1a) (corresponding stations are reported in Fig1.b): (a)  
185 on the shallow plateau (station A3; see 1 in Fig.1a). Note that station A3  
186 coincides with a site studied during the KEOPS 1 cruise, and that it was  
187 sampled twice over a 27-day period; (b) in a meander formed by a quasi-  
188 permanent retroflexion of the Polar Front (PF) and topographically-steered by  
189 the eastern escarpment (Gallieni Spur) of the Kerguelen Plateau (mainly  
190 stations E, sampled as a quasi-lagrangian temporal series) (see 2 in Fig.1a);  
191 (c) along a North-South Transect (referred to as TNS stations; see 3, grey line  
192 in Fig.1a) and a West-East Transect (referred to as TEW stations; see 4, grey



193 line in Fig.1a), both crossing the PF; and (d) in the Polar Front Zone (PFZ) in  
194 the vicinity (east) of the PF (station F-L; see 5 in Fig.1a). Furthermore we also  
195 sampled a reference HNLC/non bloom/non Fe-fertilized station southwest of  
196 the Plateau (station R-2; see 6 in Fig.1a). Station locations are given in Table  
197 1.

198 Detailed descriptions of the complex physical structure of the area,  
199 circulation, water masses and fronts are given in Park et al. (2014). Briefly,  
200 the main hydrodynamic features observed during the cruise are the following  
201 (see  $\theta$ -S diagram, Fig.2a): (1) North of the PF, stations in the PFZ (TNS-1,  
202 TEW-8 and F-L) present Antarctic Surface Waters (AASW;  $\theta \approx 4^\circ\text{C}$  and density  
203  $< 27$ );  $\theta$ -S characteristics between 150 to 400 m at station F-L (and to a  
204 lesser extent at station TNS-1) reveal the presence of interleaving with waters  
205 from northern (subantarctic) origin, centered between the 27.2 and 27.5  
206 density curves, where Antarctic Intermediate Waters (AAIW) are usually  
207 found. This contrasts with the situation at station TEW-8, where there is no  
208 evidence of interleaving; (2) stations south of the PF exhibit subsurface  
209 temperature minima characteristic of Winter Waters (WW); below the WW  
210 three water masses can be identified, namely: the Upper (temperature  
211 maximum) and Lower (salinity maximum) Circumpolar Deep Water (UCDW  
212 and LCDW), and the Antarctic Bottom Water (AABW). These water masses  
213 are present roughly in the following depth intervals:  $700 \text{ m} < \text{UCDW} < 1500 \text{ m}$ ;  
214  $1500 \text{ m} < \text{LCDW} < 2500 \text{ m}$ ;  $\text{AABW} > 2500 \text{ m}$ .

215 Based on the  $\theta$ -S characteristics (Fig.2a, -2b) and surface  
216 phytoplankton biomasses we can schematically group the stations as follows.  
217 The R-2 HNLC reference station (white dot in Fig.1b) is characterized by a  
218 very low biomass (with low iron contents; Qu erou  et al., 2015). Stations  
219 TEW-3 and TNS-8 (black dots) are characterized by a low to moderate  
220 biomass and Fe contents. Stations A3 and E-4W (red dots; south of the PF) as  
221 well as stations TNS-1, F-L and TEW-8 (blue dots; north of the PF) are

222 characterized by high biomass and iron contents. Stations in the core of the  
223 PF meander (green dots; stations TNS-6, E-1, E-2, E-3, E-4E and E-5  
224 considered as a temporal series) are characterized by moderate biomass and  
225 iron contents.

226

## 227 **2.2. Sampling and analyses**

228 22 CTD casts (surface to 500-2000 m) were sampled for particulate  
229 barium (Table 1) using a CTD-rosette equipped with 22 12L Niskin bottles.  
230 Deep particulate Ba profiles (>1000 m) were not systematically obtained from  
231 the same CTD cast, but from successive casts sampled closeby in time and  
232 space and having similar  $\theta$ -S data profiles. In the following, we use both the  
233 station and CTD numbers to refer to stations.

234 4 to 7 L of seawater were filtered onto 47 mm polycarbonate  
235 membranes (0.4  $\mu$ m porosity) under slight overpressure supplied by filtered  
236 air (0.4  $\mu$ m). The filters were rinsed with Milli-Q grade water (<5 mL) to  
237 remove sea salt, dried (50°C) and stored in Petri dishes for later analysis. In  
238 the home-based laboratory we performed a total digestion of samples using a  
239 tri-acid (0.5 mL HF/1.5 mL HCl/1 mL HNO<sub>3</sub>; all Suprapur grade) mixture in  
240 closed telfon beakers overnight at 90°C in a clean pressurized room. After  
241 evaporation close to dryness samples were re-dissolved into around 13 mL of  
242 HNO<sub>3</sub> 2%. The solutions were analysed for Ba and other major and minor  
243 elements by ICP-QMS (inductively coupled plasma-quadrupole mass  
244 spectrometry; X Series 2 ThermoFisher) equipped with a collision cell  
245 technology (CCT). To correct instrumental drift and matrix effects, internal  
246 standards and matrix-matched calibrations were used. We analysed several  
247 certified reference materials which consisted of dilute acid-digested rocks  
248 (BHVO-1, JB-3 and JGb-1), natural riverine water (SLRS-5) and multi-element  
249 artificial solutions for these external calibrations. Based on analyses of these  
250 external standards, accuracy and reproducibility are better than  $\pm$  5%. For

251 more details on sample processing and analysis we refer to Cardinal et al.  
252 (2001). Among all elements analysed, particular interest went to Ba and Al.  
253 The presence of sea-salt was checked by analysing Na and the sea-salt  
254 particulate Ba contribution was found negligible. Average detection limits  
255 equal 0.6 nM for Al and 3 pM for Ba. Detection limits were calculated as three  
256 times the standard deviation on the blank measured on board and then  
257 normalized to an average dilution factor of 385, i.e., particles from around 5 L  
258 of Milli-Q water, dissolved in a final volume of 13 mL as for the samples.  
259 Biogenic barium (hereafter called excess-Ba or  $Ba_{xs}$ ) was calculated as the  
260 difference between total particulate Ba and lithogenic Ba using Al as the  
261 lithogenic reference element (Dymond et al., 1992; Taylor and McLennan,  
262 1985). At most sites and depths the biogenic  $Ba_{xs}$  represented >95% of total  
263 particulate Ba. Lithogenic Ba reached up to 20% of total particulate Ba at  
264 some depths in the upper 80-100 m, mainly at station R-2 and stations north  
265 of the Polar Front (i.e., TEW-8, F-L and TNS-1). The standard uncertainty  
266 (Ellison et al., 2000) on  $Ba_{xs}$  data ranges between 5 and 5.5%.  $Ba_{xs}$  and Al  
267 data are reported in Appendix A.

268

### 269 **2.3. O<sub>2</sub> consumption and POC remineralization**

270 The rate of oxygen consumption and particulate organic carbon  
271 remineralization rate in the mesopelagic layer (later referred to as MR) can be  
272 estimated using an algorithm relating mesopelagic  $Ba_{xs}$  contents and oxygen  
273 consumption based on earlier observations in the Southern Ocean (Shopova  
274 et al., 1995; Dehairs et al., 1997; 2008). The detailed calculations are  
275 described in Jacquet et al. (2008a, 2011a). Briefly, we use the following  
276 equations:

$$277 \quad J_{O_2} = (Ba_{xs} - Ba_{residual})/17450 \quad (\text{Eq.1})$$

$$278 \quad C_{respired} = Z \times J_{O_2} \times RR \quad (\text{Eq.2})$$

279 where  $J_{O_2}$  is the  $O_2$  consumption ( $\mu\text{mol l}^{-1} \text{d}^{-1}$ ) and  $C_{respired}$  is the  
280 Mineralization Rate of organic carbon (in  $\text{mmol C m}^{-2} \text{d}^{-1}$ ; MR);  $Ba_{xs}$  is the  
281 depth-weighted average  $Ba_{xs}$  value (DWA<sub>v</sub>), i.e. the  $Ba_{xs}$  inventory divided by  
282 the depth layer considered  $Z$ ,  $Ba_{residual}$  is the residual  $Ba_{xs}$  signal (or  $Ba_{xs}$   
283 background) at zero oxygen consumption and RR is the Redfield C/ $O_2$  molar  
284 ratio (127/175; Broecker et al., 1985). DWA<sub>v</sub>  $Ba_{xs}$  values were calculated both  
285 for the 150 to 400 m (Plateau and deep stations) and the 150 to 800 m layers  
286 (deep stations only) (see details further below). The residual  $Ba_{xs}$  is  
287 considered as 'preformed'  $Ba_{xs}$ , left-over after partial dissolution and  
288 sedimentation of  $Ba_{xs}$  produced during a previous phytoplankton growth  
289 event. In  $BaSO_4$  saturated waters, such as the ones filling the whole ACC  
290 water column (Monnin et al. 1999), this background  $Ba_{xs}$  value was  
291 considered to reach 180 to 200 pM which is rather characteristic for the deep  
292 ocean (>1000m) (see Dehairs et al., 1997; Jacquet et al., 2008a, 2011). In  
293 the present study we used a  $Ba_{xs}$  background of 180 pM.

294 We take the opportunity here to also compare  $O_2$  consumption rates  
295 for the KEOPS 1 expedition (D. Lefèvre, unpublished data) with KEOPS 1  $Ba_{xs}$   
296 data published earlier (Jacquet et al., 2008a). No such  $O_2$  consumption data  
297 are available for KEOPS 2. During KEOPS 1, dark community respiration  
298 (DCR) was estimated from changes in the dissolved oxygen concentration  
299 over 72 hours incubations. Discrete samples were collected at three depths in  
300 the mesopelagic zone from Niskin bottles into 125  $\text{cm}^3$  borosilicate glass  
301 bottles according to the WOCE procedure, and oxygen concentration was  
302 determined by Winkler titrations using a photometric endpoint detector  
303 (Williams and Jenkinson, 1982). By integrating DCR data in the water column  
304 we estimated the rate of oxygen consumption (later referred to as  $JO_2$ -W). We  
305 compared  $JO_2$ -W obtained from incubated oxygen samples with the rate of  
306 oxygen consumption based on KEOPS 1 mesopelagic  $Ba_{xs}$  contents (Eq.1;  
307 later referred to as  $JO_2$ -Ba). Dissolved oxygen was measured three times at

308 station A3 (same location as during KEOPS2) over a 19-day period (A3 CTD  
309 #32, #74 and #119). Dissolved oxygen was also measured at station C11  
310 located off-shelf in less productive HNLC waters (51.65°S, 78.00°E; not  
311 shown in Fig.1) and was sampled two times over a 10-day period (C11  
312 CTD#42 and #83). **Fig.3 compares**  $\text{JO}_2\text{-W}$  and  $\text{JO}_2\text{-Ba}$  for repeat stations A3  
313 (#32, 74 and 119) and C11 (#42 and 83) (integration between 150-300 m).  
314  $\text{JO}_2\text{-W}$  range from 0.082 to 0.208  $\text{mmol m}^{-2} \text{d}^{-1}$  at station A3 and from 0.292  
315 to 0.528  $\text{mmol m}^{-2} \text{d}^{-1}$  at station C11. Although  $\text{JO}_2\text{-Ba}$  rates (from 0.846 to  
316 1.555  $\text{mmol m}^{-2} \text{d}^{-1}$ ) are slightly higher than  $\text{JO}_2\text{-W}$ ,  $\text{JO}_2$  rates are of the same  
317 order of magnitude and present a same trend. We observe a significant  
318 positive correlation between both  $\text{JO}_2$  rates ( $R^2=0.90$ ;  $p<0.01$ ) with a slope of  
319 0.64. The difference in oxygen consumption rates could be explained by the  
320 integration time of both methods (few hours for the incubations vs. few days  
321 to weeks for  $\text{Ba}_{\text{xs}}$ ) and by the fact that KEOPS 1 occurred at the decline of the  
322 bloom (late summer; low organic substrates), which would explain the lower  
323  $\text{JO}_2$  rates as estimated by the incubation method.

324 Overall, these results highlight the need for further constraining spatial  
325 and temporal variability of deep ocean oxygen utilisation via a combination of  
326 direct rate measurements and the  $\text{Ba}_{\text{xs}}$  proxy. In the present work  $\text{O}_2$   
327 consumption and POC remineralisation was assessed from  $\text{Ba}_{\text{xs}}$  inventories  
328 and Eqs.1 and 2. C remineralization rates are given in **Table 1**. Relative  
329 standard uncertainties (Ellison et al., 2000) on C remineralization ranged  
330 between 4 and 20%.

331

### 332 **3. RESULTS**

#### 333 **3.1. Particulate biogenic $\text{Ba}_{\text{xs}}$ profiles**

334  $\text{Ba}_{\text{xs}}$  profiles in the upper 800 m are reported in **Fig.4**. The complete  
335 whole water column data set is given in **Appendix A**. From previous studies we  
336 know that  $\text{Ba}_{\text{xs}}$  in surface waters is distributed over different, mainly non-

337 barite biogenic phases (see [Stroobants et al., 1991](#), [Jacquet et al., 2007](#),  
338 [Cardinal et al., 2005](#), [Sternberg et al., 2005](#)). As such, these do not reflect  
339 POC remineralization processes, in contrast to mesopelagic waters where  $Ba_{xs}$   
340 is mainly composed of barite ([Dehairs et al., 1980](#)) formed during prokaryotic  
341 degradation of sinking POC ([Martin et al., 1987](#); [Sarmiento et al., 1993](#);  
342 [Buesseler et al., 2007b](#)). For KEOPS 2 we observe that  $Ba_{xs}$  concentrations  
343 generally increase below 150 m (i.e., they increase above the background  
344 level set at 180 pM), but some sites have ocean surface  $Ba_{xs}$  contents  
345 significantly larger than background (E-1, 896 pM at 21 m; E4-E, 563 pM at 93  
346 m). Such values are not unusual, and very high surface values have been  
347 observed occasionally in earlier Southern Ocean studies. During KEOPS 1,  
348 surface  $Ba_{xs}$  maxima at the three A3 repeats stations ranged from 1354 to  
349 5930 pM at 50 m, likely associated with phytoplankton derived particles  
350 ([Jacquet et al., 2008a](#)).

351         The following part focuses on the mesopelagic zone where most of the  
352 remineralization of exported organic matter takes place. The  $Ba_{xs}$  profile for  
353 station R-2 (CTD #17) displayed a characteristic mesopelagic  $Ba_{xs}$  maximum  
354 reaching up to 834 pM at 304 m which is actually one of the highest values  
355 observed for the whole study ([Fig.4a](#)).  $Ba_{xs}$  profiles for stations A3 above the  
356 Kerguelen plateau (A3-1 CTD #4 and A3-2 CTD #107; [Fig.4b](#)) had lower  
357 mesopelagic  $Ba_{xs}$  contents, with values ranging from about 80 to 350 pM. For  
358 both A3 visits,  $Ba_{xs}$  values increased close to the seafloor reaching up to 1108  
359 pM (A3-1, 474 m) and 1842 pM (A3-2, 513 m). In contrast, station E-4W  
360 (located further north along the margin in deeper waters, but with similar  $\theta$ -S  
361 and Chl-a characteristics as station A3) displayed a large mesopelagic  $Ba_{xs}$   
362 maximum reaching up to 627 pM at 252 m ([Fig.4c](#)). Station TEW-3 (located  
363 on the Kerguelen plateau, in waters with similar  $\theta$ -S and Chl-a characteristics  
364 as station TNS-8) had a profile similar to the one observed at station A3-2,  
365 but compared to plateau sites A3-1 and A3-2 no increased  $Ba_{xs}$  contents were

366 observed in bottom water (Fig.4d). The other stations of the study area  
367 (Fig.4d-g) have  $Ba_{xs}$  profiles similar to the one at station E-4W, showing the  
368 characteristic  $Ba_{xs}$  maximum between 200 and 500 m. Note that for most of  
369 the stations,  $Ba_{xs}$  concentrations in waters below the mesopelagic maximum  
370 did not systematically decreased to reach the  $Ba_{xs}$  background level (180 pM;  
371 see above). In some cases  $Ba_{xs}$  contents significantly higher than residual  $Ba_{xs}$   
372 were observed until below 1000 m (see Appendix A). This is particularly  
373 salient at stations TNS-6, E-1, E-2 and F-L where  $Ba_{xs}$  values below 1000 m  
374 reach 410 pM at 1886 m (TNS-6) and 436 pM at 1498 m (E-1). These cases  
375 of high deep  $Ba_{xs}$  contents clearly contrasted with the values observed at  
376 station E4-E (Fig.4h).

377

### 378 **3.2. Depth-weighted average $Ba_{xs}$ content of mesopelagic waters**

379 Since the base of the mixed layer was generally shallower than  $\leq 150$   
380 m, this depth is taken as the upper boundary of the mesopelagic domain. The  
381 depth-weighted average (DWAV)  $Ba_{xs}$  contents, calculated for the 150-400 m  
382 and 150-800 m depth intervals, are given in Table 1. For the profiles on the  
383 plateau (500 m water column) bottom waters with evidence of sediment  
384 resuspension were not taken into account when calculating DWAV  $Ba_{xs}$  values  
385 ( $\geq 400$  m). Particle size spectra indicated that sediment resuspension occurred  
386 especially at stations A3 and TEW-3 (Jouandet et al., 2014; Lasbleiz et al.,  
387 2014; van der Merve et al., 2015;). Thus, at site A3 (Fig.4b) DWAV  $Ba_{xs}$  was  
388 calculated for the layer between 150 and 354 m for A3-1 (CTD #4) and  
389 between 150 and 405 m for A3-2 (CTD#107). For station TEW-3 (CTD #38)  
390 DWAV  $Ba_{xs}$  was calculated for the water layer between 150 and 400 m  
391 (Fig.4d). For the deep sites, we considered both, the 150-400 m and the 150-  
392 800 m depth intervals, when calculating the DWAV  $Ba_{xs}$  contents. Depth  
393 weighted average  $Ba_{xs}$  values were translated into carbon remineralization

394 rates using equation (1) and (2) given above. These rates ranged from 2 to  
395 91 mgC m<sup>-2</sup> d<sup>-1</sup> (Table 1).

396 DWAV Ba<sub>xs</sub> values range from 199 to 572 pM (Table 1) and fit within  
397 the range reported for Polar Front areas during previous studies (Cardinal et  
398 al., 2001, 2005; Jacquet et al., 2005, 2008a, 2008b, 2011; Planchon et al.,  
399 2013). For the KEOPS 2 cruise the main observed features are:

400 (a) Unexpectedly, the highest DWAV Ba<sub>xs</sub> value of the whole study area  
401 (572 pM; 150-400 m) was observed at the reference R-2 site. Bowie et al.  
402 (2014), Qu  rou   et al. (2015) and van der Merve et al. (2015) reported for R-  
403 2 local maxima in particulate and dissolved trace metals at 500 m and deeper,  
404 reflecting lateral transport of lithogenic matter possibly originating from the  
405 Leclaire Rise (a large seamount located west of R-2). Similarly, Lasbleiz et al.  
406 (2014) observed a maximum of lithogenic silica (LSi) at 500 m, confirming  
407 lithogenic inputs there. However, we note that the mesopelagic Ba<sub>xs</sub>  
408 maximum at R-2 occurs at shallower depths, around 300 m, and that there is  
409 no evidence for elevated values at 500 m where the previous authors  
410 reported higher trace element and silica concentrations. Also, as reported  
411 above (see section 2.2 and Appendix A), the higher lithogenic Ba fractions at  
412 R-2 (up to 20% of the total Ba) occur only in the upper 80 m. Moreover, we  
413 do note that surface waters at R-2 experienced already some nitrate  
414 consumption as compared to subsurface Winter Waters (Tmin waters).  
415 Indeed, surface waters had 10% less nitrate than Winter Water (26 µM at 5 m  
416 vs. 29 µM at 200 m) and the isotopic enrichment of this surface nitrate  
417 confirmed an imprint of uptake (see Dehairs et al., 2014). Also, Lasbleiz et al.  
418 (2014) report relatively low Si:C and Si:N ratios for surface ocean suspended  
419 matter) pointing to the development of a diatom assemblage just prior the  
420 sampling, consistent with the high dissolution rates of biogenic silica (BSi)  
421 Closset et al. (2014) report for R-2 surface waters. It is therefore likely that  
422 the mesopelagic Ba<sub>xs</sub> content at R-2 indeed reflects remineralization of



423 organic material that was fuelled by an important past early spring production  
424 and export event. Similarly, F. Dehairs ([unpublished results](#)) observed the  
425 presence of significant numbers of barite microcrystals in mesopelagic waters  
426 at the KERFIX time series station (50°40'S, 68°25'E) located east of R-2  
427 during late winter (Nov. 1993). Results would thus suggest the occurrence in  
428 this HNLC area of recurrent brief early spring diatom productive period pulses  
429 and subsequent export and remineralization activity in the underlying layers.  
430 Chla satellite images (Giovani online Visualization and Analysis system, NASA  
431 GES DISC) corroborate that the R-2 and KERFIX area is occasionally subject  
432 to enhanced biomass during early spring;

433 (b) The two successive visits (27-day interval) at site A3 yielded  
434 relatively low DWAV  $Ba_{xs}$  values of 267 and 316 pM, and a quite similar value  
435 was observed for the shallow station TEW-3 (324 pM), located further north  
436 on the plateau, but north of the PF. Note that for comparison purposes, we  
437 recalculated the DWAV  $Ba_{xs}$  and MR values of KEOPS 1 by considering upper  
438 and lower mesopelagic layer boundaries of 150 and 400 m rather than 125  
439 and 450 m, as in Jacquet et al. ([2008a](#)). Also, in the latter study the high  $Ba_{xs}$   
440 contents observed near the seafloor were not excluded from the calculations,  
441 while they are here. These increased benthic boundary layer  $Ba_{xs}$  contents  
442 (observed also during KEOPS 2) are due to sediment resuspension which  
443 extended up to 70 m above the seafloor during KEOPS 1 ([Blain et al., 2008](#);  
444 [Venchiarutti et al., 2008](#); [Armand et al., 2008](#)). Because of these slightly  
445 different depth intervals over which  $Ba_{xs}$  values were integrated, the KEOPS 1  
446 values discussed here will be slightly different from those reported in Jacquet  
447 et al. ([2008a](#)). [At the other depths the lithogenic Ba contribution at A3](#)  
448 [\(KEOPS 2\) was only minor](#);

449 (c) The time series stations in the Polar Front meander had DWAV  $Ba_{xs}$   
450 contents ranging from 258 to 427 pM (150-400 m), so reaching values  
451 exceeding those on the plateau. For these time series stations values

452 decreased between day 0 (TNS-6) and 12 (E-3), and then increased again at  
453 days 22 (E-4E) and 27 (E-5). Stations E-4W and TNS-8 above the plateau but  
454 in deeper waters close to the Kerguelen margin, at the edge the high biomass  
455 plume (Figure 1) had the highest DWAV  $Ba_{xs}$  values (468 and 473 pM,  
456 respectively; 150-400 m), not considering the R-2 reference station. The  
457 Polar Front F-L site, although located within the eastern part of the high  
458 biomass plume had a smaller DWAV  $Ba_{xs}$  value of 345 pM (150-400 m) and  
459 the close by station TEW-8 had the lowest DWAV  $Ba_{xs}$  value of the whole  
460 study area (199 pM; 150-400 m).

461

## 462 **4. DISCUSSION**

### 463 **4.1. Mesopelagic $Ba_{xs}$ and bacterial production**

464 Previous studies revealed that the shape of the column-integrated  
465 bacterial production (BP) profile (i.e. the attenuation length scale) was  
466 important in setting the  $Ba_{xs}$  signal in the mesopelagic zone (Dehairs et al.,  
467 2008; Jacquet et al., 2008a, 2011a). Mesopelagic  $Ba_{xs}$  content is smaller  
468 when most of the column integrated BP is restricted to the upper mixed layer  
469 (indicating an efficient, close to complete remineralization within the surface),  
470 compared to situations where a significant part of integrated BP was located  
471 deeper in the water column (reflecting significant deep bacterial activity and  
472 POC export). During KEOPS 2 the incorporation of  $^3H$ -leucine was used to  
473 estimate bacterial production. BP data are described in Christaki et al. (2014).  
474 In Fig.5 we compare column-integrated BP at 150 m over 400 m (BP150/400)  
475 and DWAV  $Ba_{xs}$  for the 150-400 m depth interval, next to the relation  
476 obtained during KEOPS 1 (BP200/125 and 150-450 m DWAV  $Ba_{xs}$ ; Jacquet et  
477 al., 2008a; Christaki et al., 2008). Excluding stations A3, E-1, E-2 and E-3,  
478 KEOPS 2 data presented a significant correlation ( $R^2=0.88$ ;  $p<0.01$ ) and a  
479 similar trend to the one reported for KEOPS 1. A similar picture was obtained  
480 when integrating DWAV  $Ba_{xs}$  and BP up to 800 m (not shown). The time series

481 "E" stations in the meander revealed a shift from stations E-1, E-2 and E-3 to  
482 stations E-4E and E-5, i.e. towards the trend reported above. A shift was also  
483 apparent at station A3 from KEOPS 2 (early spring) to KEOPS 1 (late  
484 summer). It is thus possible that results reflect the occurrence of different  
485 stage of bloom advancement. The large variability of  $Ba_{xs}$  and BP relationship  
486 during KEOPS 2, especially at A3 site and in the meander, could reflect the  
487 temporal evolution and patchiness of the establishment of mesopelagic  
488 remineralization processes in this Polar Front area.

489

#### 490 **4.2. Fate of exported organic C in the mesopelagic zone and deep** 491 **water column**

492 An important question relates to the fate of the exported POC: how  
493 much of this POC is respired in the mesopelagic waters and how much  
494 escapes remineralization and is exported to deeper layers where longer term  
495 sequestration is likely (see e.g. Passow and Carlson, 2012; [Robinson et al.,](#)  
496 [2014](#); [Schneider et al., 2008](#)). To address these questions, we defined two  
497 ratios: (1) the mesopelagic C remineralization efficiency (r-ratio in [Table 2](#))  
498 which is the ratio of mesopelagic C remineralization (MR, based on the DWAV  
499  $Ba_{xs}$  concentrations) over C export (EP) from the 150 m horizon (based on  
500  $^{234}\text{Th}$ , see [Planchon et al., 2014](#)), and (2) the C transfer efficiency at 400 and  
501 800 m (i.e., T400, T800 in [Table 2](#)) which is the fraction of C export (EP) at  
502 150 m passing through the 400 m (T400) or the 800 m (T800) horizons (e.g.,  
503  $T400 = EP400/EP150 = 1 - (MR/EP150)$ , with  $MR/EP150 = r\text{-ratio}$ ; see above).  
504 This approach is similar to the one developed by Buesseler and Boyd ([2009](#))  
505 stating that a conventional curve-fitting of particle flux data (i.e., power law  
506 or exponential) skews our interpretation of the mesopelagic processes. They  
507 recommended the use of combined metrics to capture and compare  
508 differences in flux attenuation. In the following, we compare MR fluxes for the  
509 different KEOPS 2 areas (Reference site; Plateau sites; Polar Front and Polar

510 Front Meander) and discuss remineralization and transfer efficiencies for those  
511 sites for which MR, primary production (PP) and/or EP data (Table 2) were  
512 available. PP data were estimated from uptake experiments including 24-hour  
513 incubations at different PAR levels over the euphotic layer i.e., up to the  
514 0,01% PAR level (Cavagna et al., 2014). EP data were estimated from  $^{234}\text{Th}$   
515 activities and  $^{234}\text{Th}$  /POC ratios and are discussed in Planchon et al. (2014).  
516 The thorium method integrates POC export over a 1 month period ( $^{234}\text{Th}$  half  
517 live equals 24.1 days). We remind here that MR fluxes as based on  
518 mesopelagic  $\text{Ba}_{\text{xs}}$  reflect past remineralization activity integrated over several  
519 days to a few weeks (Dehairs et al., 1997; Cardinal et al., 2005; Jacquet et  
520 al., 2007, 2008b). In order to compare EP with MR (r-ratio and transfer  
521 efficiency) we consider EP fluxes from 150 m. Results are compared with late  
522 summer KEOPS 1 results. For KEOPS 1, PP data are detailed in Lefèvre et al.  
523 (2008) and Mosseri et al. (2008), EP data are detailed in Savoye et al. (2008)  
524 and  $\text{Ba}_{\text{xs}}$  data are described in Jacquet et al. (2008a).

525

#### 526 **4.2.1. Reference station R-2**

527 Since station R-2 had the highest DWAV  $\text{Ba}_{\text{xs}}$  content it yielded the  
528 highest MR flux of the whole study area ( $91 \text{ mgC m}^{-2} \text{ d}^{-1}$ ; 150-800 m; Table  
529 2). In contrast, both PP and EP fluxes at R-2 were very low ( $132$  and  $10 \text{ mgC}$   
530  $\text{m}^{-2} \text{ d}^{-1}$ , respectively) and the calculated MR flux exceeded EP (Table 2). The  
531 resulting export efficiency (EP/PP) was high, and T400 and T800 value (the  
532 fraction of EP exported deeper than 400 m and 800 m, as defined above)  
533 equal 0 (i.e., no export of POC beyond 400 and 800 m; note that >100%  
534 values, i.e.,  $\text{MR} > \text{EP}$ , were set to zero in Fig.7a and Table 2). The fact that MR  
535 exceeds EP therefore implies a non-steady state condition at the R-2 site. As  
536 reported above, R-2 probably experienced a brief early spring diatom  
537 production pulse days to a few weeks before the start of the KEOPS 2 cruise,

538 followed by subsequent export and quite important remineralization activity in  
539 the underlying layers as depicted by MR data.

540

#### 541 **4.2.2. Station A3 on the Plateau**

542 The MR fluxes on the plateau varied little between the two visits 27  
543 days apart (Table 1) and as discussed below they were moreover similar to  
544 summer values obtained during KEOPS 1 (see Jacquet et al., 2008a) when the  
545 same A3 site was sampled 3 times over a 19-day period. While during KEOPS  
546 2 (spring) MR fluxes at A3 ranged from 11 to 14 mgC m<sup>-2</sup> d<sup>-1</sup> (with a standard  
547 uncertainty around 5%) they were slightly larger during KEOPS 1 (summer;  
548 17 to 23 mgC m<sup>-2</sup> d<sup>-1</sup>) (Fig.5). We observed differences in the mesopelagic  
549 POC remineralization efficiency between the two seasons (r-ratio, blue values  
550 in Fig.6, Table 2). During KEOPS 1 r-ratios (MR/EP) remained low, ranging  
551 from 7 to 9% of EP at A3, while during KEOPS 2 r-ratios were slightly higher  
552 but decreased from 29% (A3-1; first visit) to 13%, 27 days later (A3-2;  
553 second visit). This variation in r-ratio during KEOPS 2 is mostly due to an  
554 increase of EP (from 47 to 85 mgC m<sup>-2</sup> d<sup>-1</sup>; Planchon et al., 2014) over the  
555 same period while MR showed little change. Although at this early stage of the  
556 season (spring) PP at A3-2 had already reached 2172 mgC m<sup>-2</sup> d<sup>-1</sup> (Cavagna  
557 et al., 2014), EP remained relatively low (85 mgC m<sup>-2</sup> d<sup>-1</sup>). Here EP accounted  
558 for only about 4% of PP (low export efficiency; see green data points in  
559 Fig.5). This condition suggested that phytoplankton biomass was  
560 accumulating in the surface waters without significant export yet, or that C  
561 was channeled to higher trophic levels as suggested by Christaki et al.  
562 (2014). Note that a negative relationship between primary productivity and  
563 surface carbon export efficiency has already been reported from previous  
564 studies in the Southern Ocean (Lam et al., 2007; Morris et al., 2007; Savoye  
565 et al., 2008; Jacquet et al., 2011a, 2011b). Among possible explanations for  
566 the occurrence of high productivity-low export efficiency regimes in high

567 latitude systems Maiti et al. (2013) mentioned differences in trophic structure,  
568 grazing intensity, recycling efficiency, high bacterial activity, or increase in  
569 DOC export, but the exact reason remain unclear. In contrast, during KEOPS  
570 1 (summer), EP fluxes reached  $250 \text{ mgC m}^{-2} \text{ d}^{-1}$  at 125 m (14-31% of PP)  
571 while PP ranged from 865 to  $1872 \text{ mgC m}^{-2} \text{ d}^{-1}$ , reflecting enhanced export  
572 efficiency (Jacquet et al., 2008a; Savoye et al., 2008).

573 It is important to underline the fact that MR at station A3 was only  
574 slightly higher in summer than in spring especially considering the large  
575 differences in export efficiency between seasons. According to results from  
576 sediment traps deployed over one year at the A3 site, Rembauville et al.  
577 (2014) reported that 60% of the annual POC export at the base of the mixed  
578 layer occurred over a short periods of time representing <4% of the years  
579 and was composed by small highly silicified, fast sinking, resting spores of  
580 diatoms that bypass grazing pressure. According to these authors, the pulses  
581 are linked to nutrient depletion dynamics inducing resting spore formation.  
582 During the rest of the year, the flux was composed of small diatoms (empty  
583 frustules) and small fecal pellets, with efficient C retention in the surface layer  
584 or transfer to trophic levels. If we consider that export conditions during  
585 KEOPS 2 are more similar to those prevailing most of the year, it is surprising  
586 that during KEOPS 1 (that would reflect an export event toward the end of the  
587 growth season) MR is not more important. This would indicate that fast  
588 sinking- highly silicified- and pulsed material was directly transferred to the  
589 bottom without major remineralization. Note for example that at the complex  
590 R-2 reference station, a small export event (Laurenceau-Cornec et al.; 2015)  
591 held heavily silicified diatoms (Lasbleiz et al.; 2014), and that the material  
592 was efficiently remineralized in the upper mesopelagic layer as witnessed by  
593 the high MR values we observe for that station. For the KEOPS 2 A3 site  
594 Laurenceau-Cornec et al. (2015) report that the sinking flux collected in the  
595 upper layer using gel-filled sediment traps was composed by phytodetrital

596 aggregates that held slightly silicified diatoms (Lasbleiz et al., 2014). Even  
597 considering the shift from slightly- to highly-silicified material transfer  
598 between spring (KEOPS2) and summer (KEOPS 1), MR only slightly increases  
599 between both periods. Also, the mesozooplankton biomass at A3-2 was one of  
600 the highest of the KEOPS2 cruise, with a doubling from KEOPS 2 (early  
601 spring) to KEOPS 1 (late summer) (Carlotti et al., 2015). It is thus possible  
602 that at A3 the export event reported above, combined with a lasting grazing  
603 pressure would have induced this rather low and perduring mesopelagic  
604 remineralization. We also wonder whether the shallow water column at A3  
605 combined with lateral advection above the plateau would play a role in  
606 triggering the mesopelagic POC remineralization activity and in setting its  
607 efficiency. For KEOPS 1, Venchiarutti et al. (2008) report that lateral  
608 advection over the plateau could significantly impact particle dynamics.  
609 During KEOPS 1, station B1 (CTD68) located on the plateau upstream from A3  
610 according to the plateau circulation (Park et al., 2008) exhibited a very similar  
611  $Ba_{xs}$  distribution as station A3: low mesopelagic  $Ba_{xs}$  and important bottom  
612 resuspension (not shown here; see Jacquet et al., 2008a). These strong  
613 similarities in  $Ba_{xs}$  profiles shape would indicate that next to the pulsed nature  
614 of the events, the dynamics on the shallow plateau play an important role in  
615 limiting the extend of mesopelagic POC remineralization processes.

616 In Fig.7a is shown for both KEOPS cruises the ratio of EP over PP  
617 (export efficiency) vs. the fraction of EP exported deeper than 400m (i.e.  
618 T400; defined above). Note that for station A3-1 (KEOPS 2), there are no PP  
619 data. The A3 site shows increasing EP/PP ratios from spring (KEOPS 2) to late  
620 summer (KEOPS 1), and so do the T400 values (A3-1: 70%; A3-2: 87%;  
621 KEOPS 1 A3 site:  $92 \pm 1\%$ ). Station E-4W located in waters with similar  $\theta$ -S  
622 and Chl-a characteristics as the A3 plateau site but has a deeper water  
623 column (1384 m has PP and EP fluxes of the same order of magnitude (Table  
624 2). However, MR values ( $36 \text{ mgC m}^{-2} \text{ d}^{-1}$ ; 150-400 m) are larger at E-4W,

625 resulting in a lower T400 value of around 33%, compared to 87% for A3-2  
626 (Fig.7a). When integrating down to 800 m, T800 at E-4W equals 0 (i.e., no  
627 export of POC beyond 800 m; Fig.7a and Table 2). Station F-L (in the vicinity  
628 of the PF; 74.7°E) appears to function in a similar way as observed for E-4W  
629 (71.4°E). PP at station F-L is relatively high ( $3380 \text{ mgC m}^{-2} \text{ d}^{-1}$ ), while EP is  
630 quite low ( $43 \text{ mgC m}^{-2} \text{ d}^{-1}$ ), reflecting the fact that the biomass was not yet  
631 exported from the surface waters or was transferred to higher trophic levels.  
632 Since MR fluxes are slightly lower ( $21 \text{ mgC m}^{-2} \text{ d}^{-1}$ ; 150-400 m) at F-L than at  
633 E-4W, resulting T400 values are higher (52%) there.

634 Overall, during KEOPS 2 it appears that biomass at stations A3, E-4W  
635 and F-L (sites of high productivity) was accumulating in surface waters (e.g.  
636 transfer to higher trophic levels) and export did not start yet considering the  
637 early stage of the season during KEOPS 2. Our observations allow us to  
638 conclude the following:

639 (1) Both seasons (KEOPS 1 and KEOPS 2) showed a similar functioning of the  
640 mesopelagic ecosystem at A3. The rather low and perduring MR fluxes under  
641 high production and variable export regimes (high export efficiency during  
642 KEOPS 1 and low export efficiency during KEOPS 2) indicated that here  
643 mesopelagic remineralization does not represent a major resistance to organic  
644 matter transfer to the sea-floor at A3. On average (considering both seasons,  
645 but excluding A3-1) the C transfer efficiency into the deep (>400 m) as  
646 assessed by PP, EP and MR fluxes comparisons reached  $91 \pm 3\%$  at A3;

647 (2) In contrast to A3, E-4W and F-L showed important mesopelagic  
648 remineralization rates, reducing the efficiency of C transfer beyond 400 m to  
649 33 and 52%, respectively, and to zero for both stations beyond 800 m.  
650 Bottom depth, lateral advection, zooplankton grazing pressure and the pulsed  
651 nature of the POC transfer at A3 were the particular conditions that could  
652 drive the differences in C transfer efficiency between A3 and E4-W and F-L  
653 and limit the extend of MR processes at A3.



654

### 655 **4.3. Stations in the meander**

656 Temporal short term changes for the stations TNS-6, E-1, E-2, E-3, E-  
657 4E and E-5, located in the Polar front meander, will be discussed in this  
658 section. Note that no PP or EP data exist for TNS-6. From [Table 2](#) it appears  
659 that PP almost doubled between E-1 and E-5 but this increase was not  
660 paralleled by an increase of EP and MR, except for the 30% EP increase from  
661 E-1 to E-3. In fact overall EP shows a decreasing trend with time, while MR  
662 (150-400 m) stays rather constant, except for the decrease between E-1 and  
663 E-3 ([Table 2](#)). As reported above such a mismatch may result from  
664 differences in time scales characterizing the different processes that were  
665 compared. The most likely explanation is that in this early stage of the growth  
666 season, phytoplankton biomass was accumulating in the surface layer and  
667 export was lagging behind.

668 The ratio of EP over PP vs. T400 and T800 showed a large variability in  
669 transfer efficiency inside the meander ([Fig.7b](#)). PP and EP fluxes increased by  
670 about 30% from E-1 to E-3, but a concomitant decrease of mesopelagic MR  
671 yielded to an enhanced transfer efficiency, from 74 to 92%, through the 400  
672 m boundary and from 52 to 73% through the 800 m boundary. This suggests  
673 that significant remineralization should have occurred at greater depths (even  
674 > 1000 m) and it is also reflected by the presence of  $Ba_{xs}$  maxima below 1000  
675 m (see [Fig.4h](#) and [Appendix A](#)). This was particularly salient when plotting  
676  $Ba_{xs}$  contents vs. depths over the 27-day observation period ([Fig.8](#)). The high  
677 deep water  $Ba_{xs}$  values in [Figure 8](#) were not taken into account when  
678 integrating TNS-6 and E-1 profiles between 150 and 400 or even 150 and 800  
679 m ([Fig. 5e](#)). Considering that the seafloor in the meander area is at about  
680 2000 m depth, it seems unlikely that these high  $Ba_{xs}$  contents at depths  
681 >1000 m were due to sediment resuspension. Also, particle spectra for these  
682 sites do not reveal any bottom resuspension ([Jouandet et al., 2014; Lasbleiz](#)

683 [et al., 2014](#); [van der Merve et al., 2015](#)). Therefore, the high deep (>1000 m)  
684  $Ba_{xs}$  contents at TNS-6 and E-1 most likely reflected the fact that here  
685 significant remineralization of POC material did occur in the bathypelagic  
686 domain and even down to the sea-floor. Note that suspended particles in the  
687 depth range containing the deep  $Ba_{xs}$  maxima were dominated by the <2  $\mu$ m  
688 size fraction ([Zhou et al., pers. comm.](#)). When integrating the  $Ba_{xs}$  contents  
689 from 150 m to the sea-floor at stations TNS-6 and E-1, MR fluxes increase to  
690 156 and 184  $mgC\ m^{-2}\ d^{-1}$  respectively. Such C fluxes were similar to the EP  
691 values (maximum value of 130  $mgC\ m^{-2}\ d^{-1}$  at E-3) and suggested that the  
692 exported POC was entirely remineralized in the water column leaving no C for  
693 transfer to the sediments.

694 Overall, the temporal pattern of mesopelagic remineralization  
695 described above reflects two successive events of particle transfer: a first  
696 transfer from a previous bloom (occurred before visiting TNS-6 and perduring  
697 at E-1) and a second transfer from E-4E to E-5. The first transfer was evident  
698 by the downward (up to the bottom) propagation of the mesopelagic  $Ba_{xs}$   
699 maximum signal, which mostly weakens at E-2. The second event was  
700 reflected by the occurrence again of important mesopelagic  $Ba_{xs}$  build-up at E-  
701 4E and E-5. Overall, our results indicated the large capacity of the Polar Front  
702 Meander to transfer POC material to depth, but in contrast to station A3 on  
703 the Plateau, this transfer was coupled to intense and near to complete POC  
704 remineralization (as also observed at E-4W and F-L). Between-sites changes  
705 in mesopelagic carbon remineralization due to unequal biomass productivity  
706 and iron fertilization over the Kerguelen Plateau were thus relatively complex.  
707 Furthermore, the situation in the Meander area seems to corroborate results  
708 obtained in the iron-replete Subantarctic Zone east of the Tasman Plateau  
709 (Australian sector of the Southern Ocean; SAZ-Sense cruise; [Jacquet et al.,](#)  
710 [2011a](#), [2011b](#)), where the mesopelagic remineralization efficiency was  
711 reported relatively high (on average 91%) and the deep (>600 m) carbon

712 transfer weak (<10%). Finally, the important  $Ba_{xs}$  contents reported between  
713 1000 and 2000 m during the first stages of the meander time-series  
714 strengthen recent results indicating for the Southern Ocean that 1000 m is  
715 insufficient as an ocean-wide reference for carbon transfer and sequestration  
716 potential (Robinson et al., 2014).

717

## 718 **5. Conclusion**

719 Based on spatially and temporally well resolved mesopelagic excess  
720 particulate Ba inventories this work estimated mesopelagic POC  
721 remineralization above the Kerguelen Plateau and inside a permanent  
722 meander of the Polar Front to the east of Plateau, areas. The observed  
723 variability of mesopelagic remineralization reflects differences in the fate of  
724 the biomass that is exported to the deep ocean, between Plateau and Polar  
725 Front. Results also reveal the patchiness of the season advancement and of  
726 the establishment of remineralization processes between these sites. Our  
727 results indicate that the reference station R-2 experienced few days to weeks  
728 before the start of the cruise an export event that was efficiently  
729 remineralized in the upper mesopelagic layer. In terms of deep ocean carbon  
730 transfer efficiency, our results highlight that above the plateau (A3 site)  
731 mesopelagic remineralization is not a major barrier to organic matter transfer  
732 to the sea-floor, with carbon transfer beyond 400 m reaching up to 87% of EP  
733 during KEOPS 2, while in the Polar Front Meander remineralization of exported  
734 organic carbon in the upper 400 m is more efficient than above the plateau.  
735 In the Meander area remineralization may even balance export when including  
736 its effect in the deeper waters (till 800 m and even deeper), thus resulting in  
737 a close to zero carbon transfer to sediment. A similar condition is also  
738 observed for sites at the margin of the plateau (E-4W) and the Polar front (F-  
739 L).

740

741 **Acknowledgements**

742 We thank the officers and crew of R/V *Marion Dufresne* for their  
743 assistance during work at sea. We are indebted to chief scientist S. Blain and  
744 voyage leader B. Quéguiner for skillful leadership during the cruise and to the  
745 CTD team for managing rosette operation and CTD data. This research was  
746 supported by the French Agency of National Research grant (project KEOPS 2,  
747 #ANR-10-BLAN-0614), the Belgian Science Policy (BELSPO) project  
748 'BIGSOUTH' (SD/CA/05A), Flanders Research Foundation (FWO Project  
749 G071512N), the European Union Seventh Framework Programme (Marie Curie  
750 CIG 'MuSiCC' under grant agreement n° 294146 to D.C.) and the Strategic  
751 Research Programme at Vrije Universiteit Brussel.

752

753 **Figure captions**

754

755 Figure 1: (a) Kerguelen Island area in the Southern Ocean with KEOPS 2  
756 sampling zones and MODIS Chlorophyll concentrations ( $\text{mg m}^{-3}$ ) (Chl-a map  
757 from 11/11/2011, courtesy F. d'Ovidio) superposed. 1 refers to station A3; 2  
758 to stations E; 3 to the South-North Transect; 4 to the West-East Transect; 5  
759 to station F-L and 6 to reference station R-2; (b) Corresponding stations  
760 location. Colors indicate stations with near similar  $\theta$ -S and Chl-a  
761 characteristics.

762

763 Figure 2: (a) Potential temperature  $\theta$  - salinity S plots and isopycnals for  
764 KEOPS 2 profiles, (b) Focus on the upper 200 m water column. AASW=  
765 Antarctic Surface Waters, AAIW= Antarctic Intermediate Waters, WW= Winter  
766 Waters, UCDW and LCDW= Upper and Lower Circumpolar Deep Water,  
767 AABW= Antarctic Bottom Water. Graph constructed using Ocean Data View  
768 (Schlitzer, 2002; Ocean Data View; [http://www.awi-](http://www.awi-bremerhaven.de/GEO/ODV)  
769 [bremerhaven.de/GEO/ODV](http://www.awi-bremerhaven.de/GEO/ODV)).

770

771 Figure 3: Rates of oxygen consumption ( $\text{mmol m}^{-2} \text{d}^{-1}$ ) during KEOPS 1 as  
772 directly measured ( $\text{JO}_2\text{-W}$ ) and from mesopelagic  $\text{Ba}_{\text{xs}}$  contents ( $\text{JO}_2\text{-Ba}$ ).  
773 Rates are integrated between 150-300 m.

774

775 Figure 4: Particulate biogenic  $\text{Ba}_{\text{xs}}$  profiles (pM) in the upper 800 m (Fig.4a-g)  
776 and in the upper 2500 m (Fig.4h). Stations are identified by CTD cast  
777 numbers. BKG=  $\text{Ba}_{\text{xs}}$  background (180 pM).

778

779 Figure 5: Regression of the ratio of integrated bacterial production (BP) in the  
780 upper 150 m over integrated BP in the upper 400 m versus depth weighted  
781 average (DWA<sub>v</sub>) mesopelagic  $\text{Ba}_{\text{xs}}$  (pM; 150-400 m) during KEOPS 2. KEOPS  
782 1 data (dots) are reported for comparison.

783

784 Figure 6: Schematic, comparing the fate of POC at station A3 during KEOPS 1  
785 and KEOPS 2 cruises. PP= primary production, EP= export production at 150  
786 m depth and MR= mesopelagic POC remineralization deduced from the  $\text{Ba}_{\text{xs}}$   
787 maxima and integrated between 150-400 m; all fluxes in  $\text{mgC m}^{-2} \text{d}^{-1}$ . EP/PP  
788 (green values), MR/PP (red values) and MR/EP (r-ratio, blue values) ratios  
789 shown as %.

790

791 Figure 7: Y-axis: EP/PP = POC flux at 150 m (EP150) as a fraction of primary  
792 production (PP); X-axis: EP<sub>x</sub>/EP150 = POC flux at defined depths (EP<sub>x</sub>; here  
793 400 and 800 m) as a fraction of POC flux at 150 m (EP150). The green cross  
794 (Fig.5a) is for station A3-1 (KEOPS-2). Since no PP data is available for that  
795 station, the EP/PP value has been arbitrarily set to 0. Isolines represent the  
796 modeled 1, 5, 10, 20 and 30% of PP export to depths >at 400 or 800 m, and  
797 represent export efficiency.

798

799 Figure 8: Temporal evolution of particulate biogenic Ba ( $Ba_{xs}$ ; pM) in the  
800 upper 2000 m water column in the Polar Front meander. Graph constructed  
801 using Ocean Data View (Schlitzer, 2002; Ocean Data View; [http://www.awi-  
bremerhaven.de/GEO/ODV](http://www.awi-<br/>802 bremerhaven.de/GEO/ODV)).

803

#### 804 **Table captions**

805

806 Table 1: Station locations, CTD cast number and bottom depth during KEOPS  
807 2. Depth-weighted average values (DWA<sub>v</sub>) of mesopelagic  $Ba_{xs}$  (pM) and  $Ba_{xs}$   
808 based mesopelagic POC remineralization (MR;  $mgC\ m^{-2}\ d^{-1}$ ) integrated  
809 between 150-400 and 150-800 m depths. See text for further information on  
810 calculation.

811

812 Table 2: Comparison of mesopelagic POC remineralization (MR) with primary  
813 production (PP) and export production (EP). All fluxes in  $mg\ C\ m^{-2}\ d^{-1}$ . r-ratio  
814 is the ratio of MR over EP. EP/PP is the export efficiency. The C transfer  
815 efficiency at 400 and 800 m (T400, T800) is the fraction of C export (EP) at  
816 150 m exiting through the 400 m (T400) or the 800 m (T800) horizons. See  
817 text for further information on calculation.

818

819 Appendix A: Excess particulate biogenic Ba ( $Ba_{xs}$ ; pM) and particulate Al (nM)  
820 during KEOPS 2.

821

#### 822 **References**

823 Armand, L.K., Crosta, X., Quéguiner, B., Mosseri, J., Garcia, N. : Diatoms  
824 preserved in surface sediments of the northeastern Kerguelen Plateau,  
825 Deep- Sea Res. Pt. II, 55, 677–692, 2008.

826 de Baar, H. J. W., Boyd, P. W., Coale, K. H., Landry, M.R., Tsud, A., Assmy,  
827 P., Bakker, D.C.E, Bozec, Y., Barber, R.T., Brzezinski, M.A., Buesseler,  
828 K.O., Boyé, M., Croot, P.L., Gervais, F., Gorbunov, Y., Harrison, P.J.,  
829 Hiscock, W.T., Laan, P., Lancelot, C., Law, C.S., Levasseur, M., Marchetti,  
830 A., Millero, F.J., Nishika, J., Nojiri, Y., van Oijen, T., Riebesell, U.,  
831 Rijkenberg, M.J.A., Saito, H., Takeda, S., Timmermans, K.R., Veldhuis,  
832 J.W., Waite, A.M., Wong, C.S.: Synthesis of iron fertilization experiments:  
833 From the iron age in the age of enlightenment, *J. Geophys. Res.*, 110,  
834 C09S16, doi:10.1029/2004JC002601, 2005.

835 Blain, S., Tréguer, P., Belviso, S., Bucciarelli, E., Denis, M., Desabre, S., Fiala,  
836 M., Martin Jézéquel, V., Le Fèvre, J., Mayzaud, P., Marty, J.- C., and  
837 Razouls, S.: A biogeochemical study of the island mass effect in the  
838 context of the iron hypothesis: Kerguelen Islands, Southern Ocean, Deep-  
839 Sea Res. Pt. I, 48, 163-187, 2001.

840 Blain, S., Queguiner, B., Armand, L., Belviso, S., Bombled, B., Bopp, L.,  
841 Bowie, A., Brunet, C., Brussaard, C., Carlotti, F., Christaki, U., Corbiere,  
842 A., Durand, I., Ebersbach, F., Fuda, J. -L., Garcia, N., Gerringa, L.,  
843 Griffiths, B., Guigue, C., Guillerm, C., Jacquet, S., Jeandel, C., Laan, P.,  
844 Lefevre, D., Lo Monaco, C., Malits, A., Mosseri, J., Obernosterer, I., Park,  
845 Y. -H., Picheral, M., Pondaven, P., Remenyi, T., Sandroni, V., Sarthou, G.,  
846 Savoye, N., Scouarnec, L., Souhaut, M., Thuiller, D., Timmermans, K.,  
847 Trull, T., Uitz, J., van Beek, P., Veldhuis, M., Vincent, D., Viollier, E., Vong,  
848 L., and Wagener, T.: Effect of natural iron fertilization on carbon  
849 sequestration in the Southern Ocean, *Nature*, 446, 1070-1074, 2007.

850 Blain, S., Quéguiner, B., and Trull, T.: The natural iron fertilization experiment  
851 keeps (kerguelen ocean and plateau compared study): An overview,  
852 *Deep-Sea Res. Pt. II*, 55, 559–565, 2008.

853 Boyd, P. W., Bakker, D. C. E., Chandler, C.: A new database to explore the  
854 findings from large-scale ocean iron enrichments experiments,  
855 *Oceanography*, 25, 64–71, doi:10.5670/oceanog.2012.104, 2012.

856 Boyd, P. W., Law, C. S., Wong, C. S., Nojiri, Y., Tsuda, A., Levasseur, M.,  
857 Takeda, S., Rivkin, R., Harrison, P. J., Strzepek, R., Gower, J., McKay, R.  
858 M., Abraham, E., Arychuk, M., Barwell-Clarke, J., Crawford, W., Crawford,  
859 D., Hale, M., Harada, K., Johnson, K., Kiyosawa, H., Kudo, I., Marchetti,  
860 A., Miller, W., Needoba, J., Nishioka, J., Ogawa, H., Page, J., Robert, M.,  
861 Saito, H., Sastri, A., Sherry, N., Soutar, T., Sutherland, N., Taira, Y.,  
862 Whitney, F., Wong, S. K. E., and Yoshimura, T.: The decline and fate of an  
863 iron-induced subarctic phytoplankton bloom, *Nature*, 428, 549–553, 2004.

864 Boyd, P. W., Watson, A. J., Law, C. S., Abraham, E. R., Trull, T., Murdoch, R.,  
865 Bakker, D. C. E., Bowie, A. R., Buesseler, K. O., Chang, H., Charette, M.,  
866 Croot, P., Downing, K., Frew, R., Gall, M., Hadfield, M., Hall, J., Harvey,  
867 M., Jameson, G., LaRoche, J., Liddicoat, M., Ling, R., Maldonado, M. T.,  
868 McKay, R. M., Nobber, S., Pickmere, S., Pridmore, R., Rintoul, S., Safi, K.,  
869 Sutton, P., Strzepek, R., Tanneberger, K., Turner, S., Waite, A., and  
870 Zeldis, J.: Phytoplankton bloom upon mesoscale iron fertilization of polar  
871 Southern Ocean water, *Nature*, 407, 695–702, 2000.

872 Bowie, A. R., van der Merwe, P., Qu  rou  , F., Trull, T., Fourquez, M.,  
873 Planchon, F., Sarthou, G., Chever, F., Townsend, A. T., Obernosterer, I.,  
874 Sall  e, J.-B., and Blain, S.: Iron budgets for three distinct biogeochemical  
875 sites around the Kerguelen archipelago (Southern Ocean) during the  
876 natural fertilisation experiment KEOPS-2, *Biogeosciences Discuss.*, 11,  
877 17861-17923, doi:10.5194/bgd-11-17861-2014, 2014.

878 Broecker, W. S., Takahashi, T., Takahashi, T.: Sources and flow patterns of  
879 deep-ocean waters as deduced from potential temperature, salinity and  
880 initial phosphate concentration, *J. Geophys. Res.*, 90, 6925-6939, 1985.



881 Buesseler, K. O., Andrews, J.E., Pike, S.M., Charette, M.A.: The effect of iron  
882 fertilization on carbon sequestration in the Southern Ocean, *Science*, 304,  
883 414– 417, 2004.

884 Buesseler, K.O., Andrews, J.E., Pike, S.M., Charette, M.A., Goldson, L.E.,  
885 Brzezinski, M.A., Lance, V.P.: Particle export during the Southern Ocean  
886 Iron Experiment (SOFeX), *Limnol. Oceanogr.*, 50 (1), 311– 327, 2005.

887 Buesseler, K.O., Antia, A.N., Chen, M., Fowler, S.W., Gardner, W.D.,  
888 Gustaffson, Ö., Harada, K., Michaels, A.F., Rutgers van der Loeff, M.,  
889 Sarin, M., Steinberg, D.K., Trull, T.: An assessment of the use of sediment  
890 traps for estimating upper ocean particle fluxes. *Journal of Marine*  
891 *Research*, 65(3): 345-416, 2007a.

892 Buesseler, K.O., Lamborg, C.H., Boyd, P.W., Lam, P.J., Trull, T.W., Bidigare,  
893 R.R., Bishop, J. K. B., K.L., Casciotti, Dehairs, F. , Elskens, M. , Honda,  
894 M. , Karl, D. M., Siegel, D. A., Silver, M. W., Steinberg, D.K. , Valdes, J.,  
895 Van Mooy, B. , Wilson, S. : Revisiting carbon flux through the ocean's  
896 twilight zone, *Science*, 316, 567–569, 2007b.

897 Buesseler, K.O., and Boyd, P.W.: Shedding light on processes that control  
898 particle export and flux attenuation in the twilight zone. *Limnol.*  
899 *Oceanogr.*, 54 (4), 1210-1232, 2009.

900 Cardinal, D., Dehairs, F., Cattaldo, T., and André, L.: Constraints on export  
901 and advection in the Subantarctic and Polar Front Zones, south of  
902 Australia from the geochemistry of suspended particles, *J. Geophys. Res.-*  
903 *Oceans*, 106, 31637-31656, doi : 10,1029/2000JC000251, 2001

904 Cardinal, D., Savoye, N., Trull., T.W., André, L., Kopczynska, E., Dehairs, F.,  
905 2005. Particulate Ba distributions and fluxes suggest latitudinal variations  
906 of carbon mineralization in the Southern ocean, *Deep-Sea Res. Pt. I*, 52,  
907 355-370, 2005.

908 Carlotti, F., Jouandet, M.-P., Nowaczyk, A., Harmelin-Vivien, M., Lefèvre, D.,  
909 Guillou, G., Zhu, Y., Zhou, M. : Mesozooplankton structure and functioning

910 during the onset of the Kerguelen Bloom during Keops2 survey,  
911 *Biogeosciences Discuss.*, 12, 2381-2427, doi:10.5194/bgd-12-2381-2015,  
912 2015.

913 Cavagna, A. J., Fripiat, F., Elskens, M., Dehairs, F., Mangion, P.,  
914 Chirugien, L., Closset, I., Lasbleiz, M., Flores-Leiva, L., Cardinal, D.,  
915 Leblanc, K., Fernandez, C., Lefèvre, D., Oriol, L., Blain, S., and  
916 Quéguiner, B.: Biological productivity regime and associated N cycling in  
917 the vicinity of Kerguelen Island area, Southern Ocean, *Biogeosciences*  
918 *Discuss.*, 11, 18073-18104, doi:10.5194/bgd-11-18073-2014, 2014.

919 Closset, I., Lasbleiz, M., Leblanc, K., Quéguiner, B., Cavagna, A.-J., Elskens,  
920 M., Navez, J., and Cardinal, D.: Seasonal evolution of net and  
921 regenerated silica production around a natural Fe-fertilized area in the  
922 Southern Ocean estimated from Si isotopic approaches, *Biogeosciences*,  
923 11, 5827-5846, doi: 10.5194/bg-11-5827-2014, 2014.

924 Christaki, U., Obernosterer, I., VanWambeke, F., Veldhuis, M., Garcia, N., and  
925 Catala, P.: Microbial food web structure in a naturally iron fertilized area in  
926 the southern ocean (Kerguelen plateau), *Deep-Sea Res. Pt. II*, 55, 706–  
927 719, 2008.

928 Christaki, U., Lefèvre, D., Geoges, C., Colombet, J., catala, P., Courties, C.,  
929 Sime-Ngando, T., Blain, S., and Obernosterer, I.: Microbial food web  
930 dynamics during spring phytoplankton blooms in the naturally iron-  
931 fertilized Kerguelen area (Southern Ocean), *Biogeosciences*, 11, 6739–  
932 3753, doi:10.5194/bg-11-6739-2014, 2014.

933 Dehairs, F., Chesselet, R., Jedwab, J.: Discrete suspended particles of barite  
934 and the barium cycle in the open ocean, *Earth Planet. Sc. Lett.*, 49, 40-42,  
935 1980.

936 Dehairs, F., Baeyens, W., Goeyens, L.: Accumulation of suspended barite at  
937 mesopelagic depths and export production in the Southern Ocean, *Science*,  
938 258, 1332–1335, 1992.

939 Dehairs, F., Shopova, D., Ober, S., Veth, C., Goeyens, L.: Particulate barium  
940 stocks and oxygen consumption in the Southern Ocean mesopelagic water  
941 column during spring and early summer: Relationship with export  
942 production, *Deep-Sea Res. Pt II*, 44, 497-516, 1997.

943 Dehairs, F., Jacquet, S.H.M., Savoye, N., van Mooy, B., Buesseler, K., Bishop,  
944 J., Lamborg, C., Elskens, M., Baeyens, W., Casciotti K., Monnin , C.:  
945 Barium in twilight zone suspended matter as proxy for organic carbon  
946 mineralization: results for the North Pacific, *Deep-Sea Res. Pt. II*, 55,  
947 1673-1683, 2008.

948 Dehairs, F., Fripiat, F., Cavagna, A.-J., Trull, T. W., Fernandez, C., Davies, D.,  
949 Roukaerts, A., Fonseca Batista, D., Planchon, F., and Elskens, M.: Nitrogen  
950 cycling in the Southern Ocean Kerguelen Plateau area: evidence for  
951 significant surface nitrification from nitrate isotopic compositions,  
952 *Biogeosciences Discuss.*, 11, 13905-13955, doi:10.5194/bgd-11-13905-  
953 2014, 2014.

954 D'ovidio, F., Della Penna, A., Trull, T.W., Nencioli, F., Pujol, I., Rio, M.H., Park,  
955 Y.H., Cotté, C., Zhou, M., Blain, S.: The biogeochemical structuring role of  
956 horizontal stirring: Lagrangian perspectives on iron delivery downstream of  
957 the Kerguelen plateau, *Biogeosciences Discuss.*, 12, 779-814,  
958 doi:10,5194/bdg-12-779-2015, 2015.

959 Dymond, J.R., Suess, E., Lyle, M.: Barium in deep-sea sediment: a  
960 geochemical proxy for paleoproductivity, *Paleoceanography*, 7, 163-181,  
961 1992.

962 Ellison, Eurachem/CITAC Guide CG4, Quantifying Uncertainty in Analytical  
963 Measurement. Eds. S.L.R. Ellison, M. Rosslein and A. Williams. Second  
964 edition ISBN 0948926 15 5, Pp 120, 2000.

965 François, R., Honjo, S., Krishfield, R., and Manganini, S.: Factors controlling  
966 the flux of organic carbon to the bathypelagic zone of the ocean, *Global*  
967 *Biogeochem. Cy.*, 16(4), 1087 doi:10.1029/2001GB001722, 2002.

968 Gervais, F., Riebesell, U., Gorbunov, M. Y.: Changes in primary productivity  
969 and chlorophyll a in response to iron fertilization in the southern Polar  
970 Frontal Zone, *Limnol. Oceanogr.*, 47, 1324–1335, 2002.

971 Henson, S. A., et al. (2011), A reduced estimate of the strength of the  
972 ocean's biological carbon pump, *Geophys. Res. Lett.*, 38(4), L04606.

973 Hoffmann, L., Peeken, I., Lochte, K., Assmy, P., Veldhuis, M.: Different  
974 reactions of Southern Ocean phytoplankton size classes to iron  
975 fertilization, *Limnol. Oceanogr.*, 51, 1217–1229, 2006.

976 Jacquet, S.H.M., Dehairs, F., Cardinal, D., Navez, J., Delille, B.: Barium  
977 distribution across the Southern Ocean Frontal system in the Crozet-  
978 Kerguelen Basin, *Mar. Chem.*, 95(3-4), 149-162, 2005.

979 Jacquet, S.H.M., Dehairs, F., Elskens, M., Savoye, N., Cardinal, D.: Barium  
980 cycling along WOCE SR3 line in the Southern Ocean, *Mar. Chem.*, 106, 33-  
981 45, 2007.

982 Jacquet, S.H.M., Dehairs, F., Savoye, N., Obernosterer, I., Christaki, U.,  
983 Monnin, C., Cardinal, D.: Mesopelagic organic carbon mineralization in the  
984 Kerguelen Plateau region tracked by biogenic particulate Ba, *Deep-Sea*  
985 *Res. Pt. II*, 55 (5-7), 868-879, 2008a.

986 Jacquet, S.H.M., Savoye, N., Dehairs, F., Strass, V., Cardinal, D.: Mesopelagic  
987 carbon mineralization during the European Iron Fertilization Experiment  
988 (EIFEX), *Glob. Biogeochem. Cy.*, 22, GB1023,  
989 doi:10.1029/2006GB002902, 2008b.

990 Jacquet, S.H.M., Dehairs, F., Becquevort, S., Dumont, I., Cavagna, A.,  
991 Cardinal, D.: Twilight zone organic carbon remineralization in the PFZ and  
992 SAZ south of Tasmania (Southern Ocean), *Deep-Sea Res. Pt. II*, 58 (22-  
993 21), 2222-2234 doi:10.1016/j.dsr2.2011.05.029, 2011a.

994 Jacquet, S.H.M., Lam, P., Trull, T., Dehairs, F.: Carbon export production in  
995 the Polar front zone and Subantarctic Zone south of Tasmania, *Deep-Sea*

996 Res. Pt. II, 58 (21-22), 2277-2292 doi:10.1016/j.dsr2.2011.05.035,  
997 2011b.

998 Jouandet, M.P., Jackson, G.A., Carlotti, F., Picheral, M., Stemmann, L., and  
999 Blain, S., Rapide formation of large aggregates during the spring bloom of  
1000 Kerguelen Island: observation and model comparisons, *Biogeosciences*,  
1001 11, 4393-4406, doi:10.5194/bg-11-4393-2014, 2014 .

1002 Lam, P. J., and Bishop, J. K. B.: High biomass, low export regimes in the  
1003 Southern Ocean, *Deep-Sea Research II*, 54, 601-638, 2007.

1004 Lampitt, R. S., Achterberg, E.P., Anderson, T.R., Hughes, J.A., Iglesias-  
1005 Rodriguez, M.D., Kelly-Gerreyn, B.A., Lucas, M., Popova, E.E., Sanders,  
1006 R., Shepherd, J.G., Smythe-Wright, D., Yool, A. : Ocean fertilization: A  
1007 potential means of geoengineering?, *Philos. Trans. R. Soc. A*, 366, 3919–  
1008 3945, doi:10.1098/rsta.2008.0139, 2008.

1009 Lampitt, R. S., Antia, A.N.: Particle flux in deep seas: regional characteristics  
1010 and temporal variability, *Deep-Sea Res. Pt I*, 44, 1377-1403, 1997.

1011 Lasbleiz, M., Leblanc, K., Blain, S., Ras, J., Cornet-Barthaux, V., Hélias  
1012 Nunige, S., and Quéguiner, B.: Pigments, elemental composition (C, N, P,  
1013 and Si), and stoichiometry of particulate matter in the naturally iron  
1014 fertilized region of Kerguelen in the Southern Ocean, *Biogeosciences*, 11,  
1015 5931–5955, doi:10.5194/bg-11- 5931-2014, 2014.

1016 Laurenceau-Cornec, E. C., Trull, T. W., Davies, D. M., Bray, S. G., Doran, J.,  
1017 Planchon, F., Carlotti, F., Jouandet, M.-P., Cavagna, A.-J., Waite, A. M.,  
1018 and Blain, S.: The relative importance of phytoplankton aggregates and  
1019 zooplankton fecal pellets to carbon export: insights from free-drifting  
1020 sediment trap deployments in naturally iron-fertilised waters near the  
1021 Kerguelen plateau, *Biogeosciences*, 12, 1007-1027, doi:10.5194/bg-12-  
1022 1007-2015, 2015.

1023 Laws, E. A., et al. (2000), Temperature effects on export production the  
1024 ocean, *Global Biogeochem. Cycles*, 14(4), 1231–1246.

1025 Lefèvre, D., Guigue, C., Obernosterer, I.: The metabolic balance at two  
1026 contrasting sites in the Southern Ocean: the iron-fertilized Kerguelen area  
1027 and HNLC waters, *Deep-Sea Res. Pt. II*, 55, 766–776,  
1028 doi:10.1016/j.dsr2.2007.12.006, 2008.

1029 Le Moigne, F. A. C., Moore, C. M., Sanders, R. J., Villa-Alfageme, M.,  
1030 Steigenberger, S., and Achterberg, E. P.: Sequestration efficiency in the  
1031 iron-limited North Atlantic: Implications for iron supply mode to fertilized  
1032 blooms, *Geophys. Res. Lett.*, 41, doi:10.1002/2014GL060308, 2014.

1033 Longhurst, A.R., Bedo, A.W., Harrison, W.G., Head, E.J.H., Sameoto, D.D. :  
1034 Vertical flux of respiratory carbon by oceanic diel migrant biota, *Deep-Sea*  
1035 *Res Pt*, 37 (4), 685–694, 1990.

1036 Maiti, K., Charette, M., Buesseler, K., and Kahru, M.: An inverse relationship  
1037 between production and export efficiency in the Southern Ocean, *Geophys.*  
1038 *Res. Lett.*, 40, 2013.

1039 Martin, J.H., Knauer, G.A., Karl, D.M., Broenkow, W.W.: VERTEX: carbon  
1040 cycling in the NE Pacific, *Deep-Sea Res.*, 34, 267–285, 1987.

1041 Monnin, C., Jeandel, C., Cattaldo, T., Dehairs, F.: The marine barite saturation  
1042 state of the world's oceans, *Mar. Chem.*, 65(3-4), 253-261, 1999.

1043 Morris, P.J, and Charette, M.A.: A synthesis of upper ocean carbon and  
1044 dissolved iron budgets for Southern Ocean natural iron fertilization studies  
1045 (2013), *Deep-Sea Res.*, 90, 147-157, 2013.

1046 Passow, U., Carlson, C. A. : The biological pump in a high CO<sub>2</sub> world, *Mar.*  
1047 *Ecol. Prog. Ser.*, 470, 249–271, doi:10.3354/meps09985, 2012.

1048 Porris, P.J., Sanders, R., Turnewitsch, R., Thomalla, S., 234<sup>Th</sup>-derived  
1049 particulate organic carbon export from an island-induced phytoplankton  
1050 bloom in the Southern Ocean, *Deep-Sea Res. Pt. II*, 24, 2208-2232, 2007

1051 Mosseri, J., Quéguiner, B., Armand, L. K., and Cornet-Barthaux, V.: Impact of  
1052 iron on silicon utilization by diatoms in the Southern Ocean: a case study

1053 of Si/ N cycle decoupling in a naturally iron-enriched area, *Deep-Sea Res.*  
1054 Pt. II, 55, 801-819, doi :10.1016/j.dsr2,2007,12,003, 2008.

1055 Park, Y. H., Durand, I., Kestenare, E., Rougier, G., Zhou, M., d'Ovidio, F.,  
1056 Cotté, C., and Lee J. H.: Polar front around the Kerguelen islands: An up-  
1057 to-date determination and associated circulation of surface/subsurface  
1058 water. *J. Geophys. Res. Oceans*, 119, i10.1002/2014JC010061, 2014.

1059 Park, Y.-H., Roquet, F., Durand, I., and Fuda, J.-L.: Large-scale circulation  
1060 over and around the Northern Kerguelen Plateau, *Deep-Sea Res. Pt. II*, 55,  
1061 566–581, doi:10.1016/j.dsr2.2007.12.030, 2008.

1062 Planchon, F., Cavagna A.J., Cardinal, D., André, L., Dehairs, F. Late summer  
1063 particulate organic carbon export and twilight zone remineralisation in the  
1064 Atlantic sector of the Southern Ocean, *Biogeosciences*, 10, 803–820,  
1065 doi:10.5194/bg-10-803-2013, 2013.

1066 Planchon, F., Ballas, D., Cavagna A. J., Van Der Merwe, P., Bowie, A., Trull,  
1067 T., Laurenceau-Cornec, E., Davis, D., and Dehairs, F.: Carbon export in  
1068 the naturally iron fertilized Kerguelen area of the Southern Ocean using  
1069 <sup>234</sup>Th-based approach, *Biogeosciences Discuss.*, 11, 15991-16032,  
1070 doi:10,5194/bgd-11-15991-2014, 2014.

1071 Pollard, R. T., Salter, I., Sanders, R. J., Lucas, M. I., Moore, C. M., Mills, R. A.,  
1072 Statham, P. J., Allen, J. T., Baker, A. R., Bakker, D. C. E., Charette, M. A.,  
1073 Fielding, S., Fones, G. R., French, M., Hickman, A. E., Holland, R. J.,  
1074 Hughes, J. A., Jickells, T. D., Lampitt, R. S., Morris, P. J., Nedelec, F. H.,  
1075 Nielsdottir, M., Planquette, H., Popova, E. E., Poulton, A. J., Read, J. F.,  
1076 Seeyave, S., Smith, T., Stinchcombe, M., Taylor, S., Thomalla, S.,  
1077 Venables, H. J., Williamson, R., and Zubkov, M. V.: Southern Ocean deep-  
1078 water carbon export enhanced by natural iron fertilization, *Nature*, 457,  
1079 577-U581, Doi 10.1038/Nature07716, 2009.

1080 Quéroué, F., Sarthou, G., Planquette, H. F., Bucciarelli, E., Chever, F.,  
1081 van der Merwe, P., Lannuzel, D., Townsend, A. T., Cheize, M., Blain, S.,

1082 d'Ovidio, F., and Bowie, A. R.: High variability of dissolved iron  
1083 concentrations in the vicinity of Kerguelen Island (Southern Ocean),  
1084 Biogeosciences Discuss., 12, 231-270, doi:10.5194/bgd-12-231-2015,  
1085 2015.

1086 Rembauville, M., Blain, S., Armand, L., Quéguiner, B., and Salter, I.: Export  
1087 fluxes in a naturally fertilized area of the Southern Ocean, the Kerguelen  
1088 Plateau: ecological vectors of carbon and biogenic silica to depth (Part 2),  
1089 Biogeosciences Discuss., 11, 17089-17150, doi:10.5194/bgd-11-17089-  
1090 2014, 2014.

1091 Robinson, J., Popova, E. E., Yool, A., Srokosz, M. A., Lampitt, R. S., and  
1092 Blundell, J. R.: How deep is deep enough? Ocean iron fertilization and  
1093 carbon sequestration in the Southern Ocean, Geophys. Res. Lett., 41,  
1094 2489-2495, 2014.

1095 Salter, I., Lampitt, R.S., Sanders, R., Poulton, A., Kemp, A.E.S., Boorman, B.,  
1096 Saw, K., Pearce, R.: Estimating carbon, silica and diatom export from a  
1097 naturally fertilised phytoplankton bloom in the Southern Ocean using  
1098 PELAGRA: a novel drifting sediment trap, Deep-Sea Res. Pt. II, 54, 2233-  
1099 2259, 2007.

1100 Sarmiento, J.L., Slater, R.D., Fasham, M.J.R., Ducklow, H.W., Toggweiler,  
1101 J.R.: A seasonal three-dimensional ecosystem model of nitrogen cycling in  
1102 the North Atlantic photic zone, Global Biogeochem. Cy., 7, 417-450, 1993.

1103 Savoye, N., Trull, T., Jacquet, S.H.M., Navez, J., Dehairs, F.: <sup>234</sup>Th-derived  
1104 export fluxes during a natural iron fertilization experiment (KEOPS), Deep-  
1105 Sea Res. Pt. II, 55 (5-7), 841-855, 2008.

1106 Schlitzer, R., Ocean Data View, <http://www.awi-bremerhaven.de/GEO/ODV>,  
1107 2002.

1108 Schneider, B., Bopp, L., Gehlen, M.: Assessing the sensitivity of modeled  
1109 airsea CO<sub>2</sub> exchange to the remineralization depth of particulate organic



1110 and inorganic carbon, *Global Biogeochem. Cy.*, 22, GB3021, doi:10.1029/  
1111 2007GB003100, 2008.

1112 Shopova, D., Dehairs, F., Baeyens, W.: A simple model of biogeochemical  
1113 element distribution in the oceanic water column, *J. Mar. Sy.*, 6, 331–344,  
1114 1995.

1115 Smetacek, V., Klass, C., Strass, V.H., Assmy, P., Montresor, M., Cisewski, B.,  
1116 Savoye, N., Webb, A., d'Ovidio, F., Arrieta, J.M., Bathmann, U., Bellerby,  
1117 R., Mine Berg, G., Croot, P., Gonzalez, S., Jenjes, J., Herndl, G.J.,  
1118 Hoffmann, L.J., Leach, H., Losh, M., Mills, M.M., Neill, C., Peeken, I.,  
1119 Rottgers, R., Sachs, O., Sauter, E., Schmidt, M.M., Schwarz, J.,  
1120 Terbruggen, A., Wolf-Gladrow, D. : Deep carbon export from a Southern  
1121 Ocean iron-fertilized diatom bloom, *Nature*, 487, 313–319,  
1122 doi:10.1038/nature11229, 2012.

1123 Sternberg, E., Jeandel, C., Miquel, J.-C., Gasser, B., Souhaut, M., Arraes-  
1124 Mescoff, R., Francois R. : Particulate barium fluxes and export production  
1125 in the northwestern Mediterranean. *Mar. Chem.* 105, 281–295, 2007.

1126 Sternberg, E., Jeandel, C., Robin, E., Souhaut, M.: Seasonal cycle of  
1127 suspended barite in the Mediterranean Sea, *Geochimica et Cosmochimica*  
1128 *Acta*, 72, 4020-4034, 2008a.

1129 Sternberg, E., Tang, D., Ho, T.-Y., Jeandel, C., Morel, M.M.: Barium uptake  
1130 and adsorption in diatoms, *Geochimica et Cosmochimica Acta*, 69, 11,  
1131 2745-2752, 2008b.

1132 Strass, V., Cisewski, B., Gonzales, S., Leach, H., Loquay, K.-D., Prandke, H.,  
1133 Rohr, H., Thomas, M.: The physical setting of the European Iron  
1134 Fertilization Experiment 'EIFEX' in the Southern Ocean, *Reports on Polar*  
1135 *and Marine Research*, 500, 15–49, 2005.

1136 Stroobants, N., Dehairs, F., Goeyens, L., Vanderheijden, N., Van Grieken, R.:  
1137 Barite formation in the Southern Ocean water column, *Mar. Chem.*, 35,  
1138 411-422, 1991.

1139 Taylor, S.R., McLennan, S.M.: The continental crust: its composition and  
1140 evolution, Blackwell Scientific Publications, 312pp, 1985.

1141 van der Merwe, P., Bowie, A. R., Qu  rou  , F., Armand, L., Blain, S.,  
1142 Chever, F., Davies, D., Dehairs, F., Planchon, F., Sarthou, G.,  
1143 Townsend, A. T., and Trull, T.: Sourcing the iron in the naturally-fertilised  
1144 bloom around the Kerguelen Plateau: particulate trace metal dynamics,  
1145 *Biogeosciences*, 12, 739-755, doi:10.5194/bg-12-739-2015, 2015.

1146 Venchiarutti, C., Jeandel, C., Roy-Barman, M.: Particle dynamics study in the  
1147 wake of Kerguelen Island using thorium isotopes, *Deep-Sea Res. Pt. I*, 55,  
1148 1343-1363, 2008.

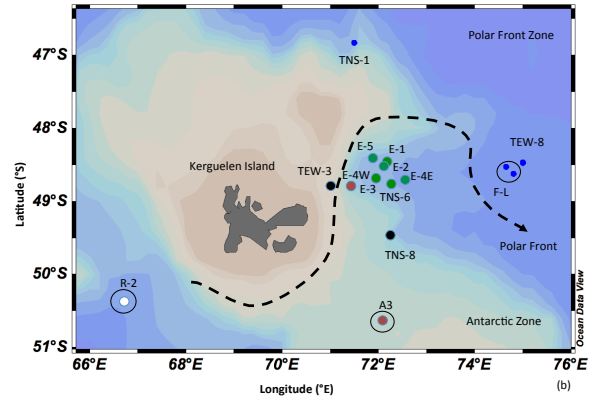
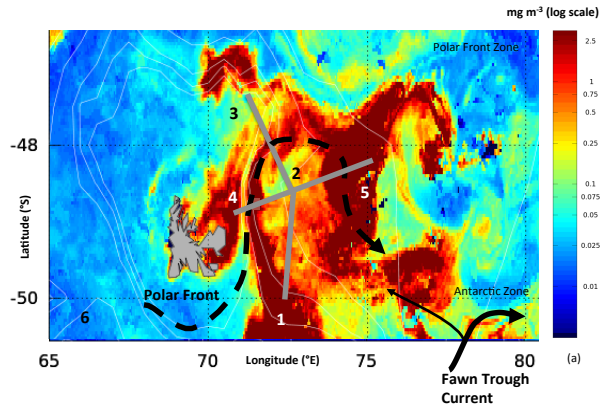
1149 Williams, P.J., Jenkinson, N.W. : A transportable microprocessor-controlled  
1150 precise Winkler titration suitable for field station and shipboard use.  
1151 *Limnol. Oceanogr.* 27, 576-585, 1982.

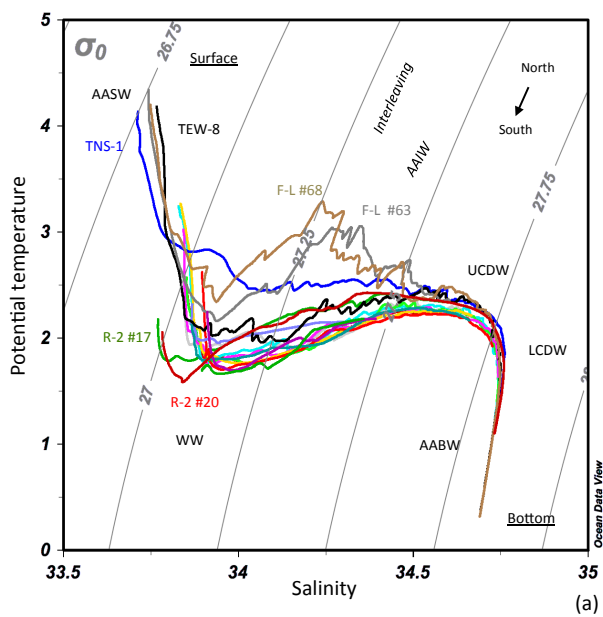
1152 Zhou, M., Zhu, Y., Dorland, R.D., Measures, C.I.: Dynamics of the current  
1153 system in the southern Drake Passage, *Deep-Sea Res. Pt I*, 57, 1039-  
1154 1048, 2010.

1155 Zhou, M., Zhu, Y., Measures, C.I., Hatta, M., Charette, M.A., Gille, S.T.,  
1156 Frants, M., Jiang, M., Mitchell, B.G.: Winter mesoscale circulation on the  
1157 shelf slope region of the southern Drake Passage, *Deep-Sea Res. Pt II*, 90,  
1158 4-14, 2013.

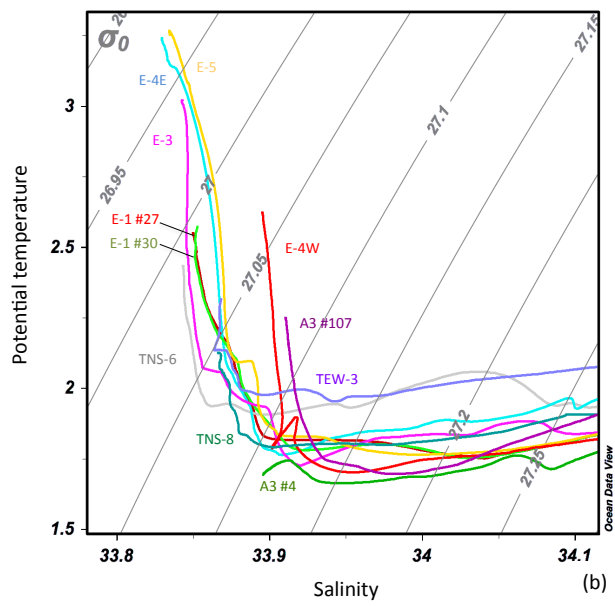
1159

1160



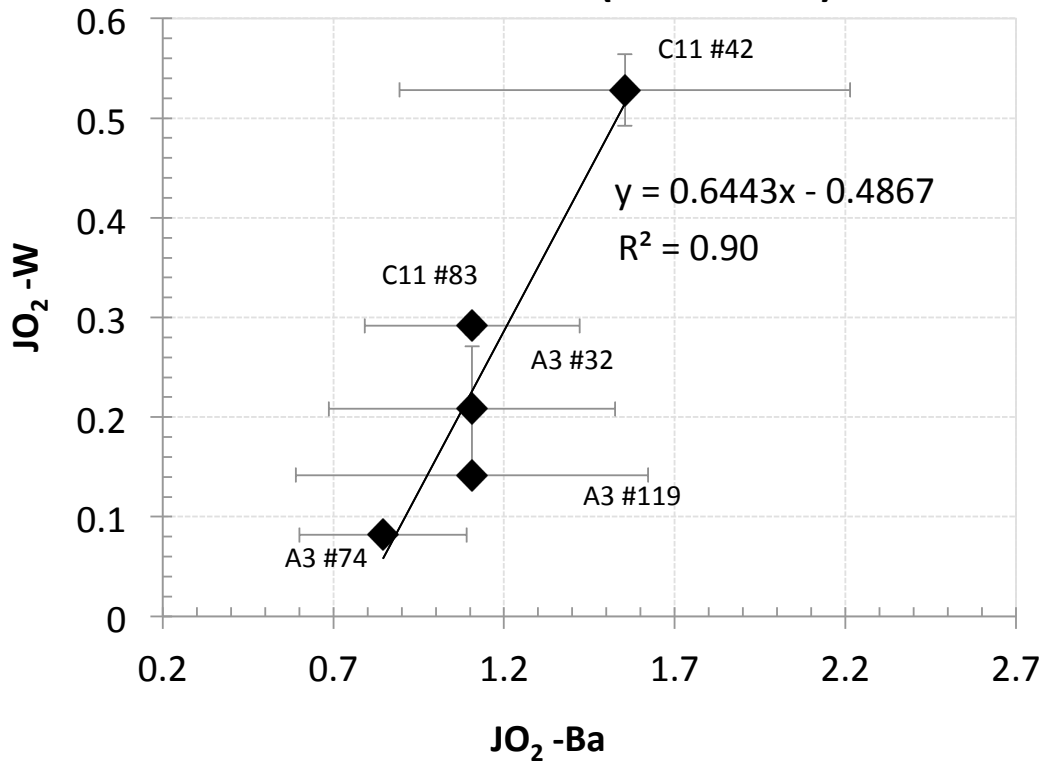


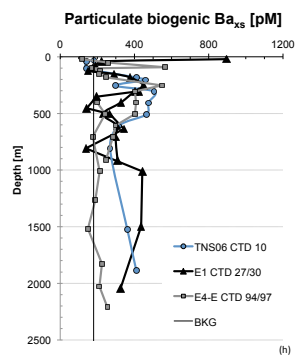
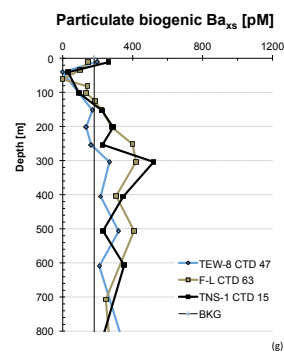
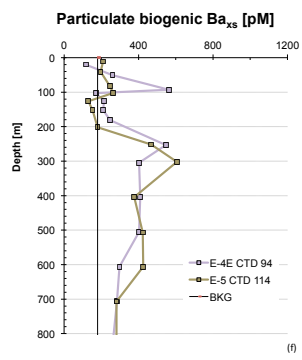
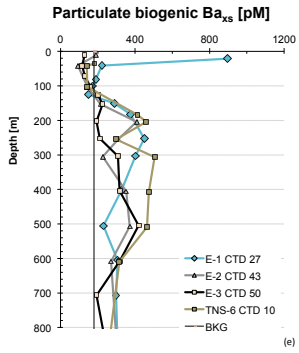
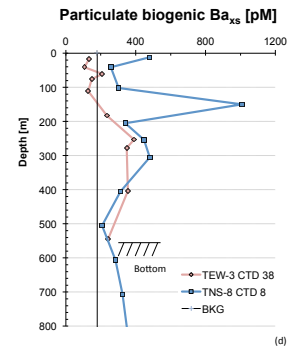
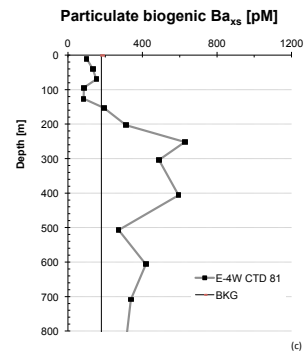
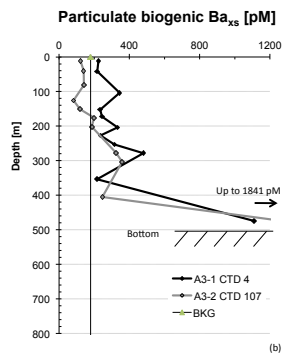
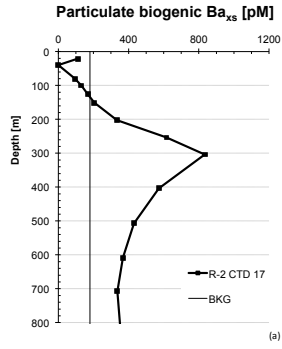
(a)

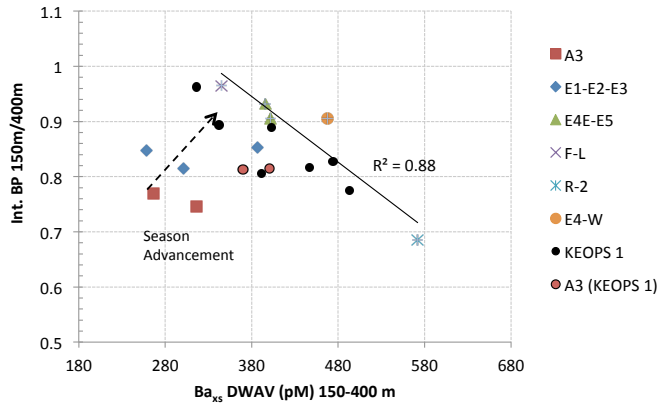


(b)

mmol m<sup>2</sup> d<sup>-1</sup> (150-300 m)







**KEOPS 2  
(Early spring 2011)**

**KEOPS 1  
(Late summer 2005)**

	<b>A3-1</b>	<b>A3-2</b>	<b>Mean of the 3 repeats</b>
PP	Not available	2172	864-1872
	↓ -	↓ 4%	↓ 14-31%
EP	47	85	250
	↓ 29%	↓ 13%	↓ 7-9%
MR	14	11	17-23
	↓ -	↓ <1%	↓ 1-2%

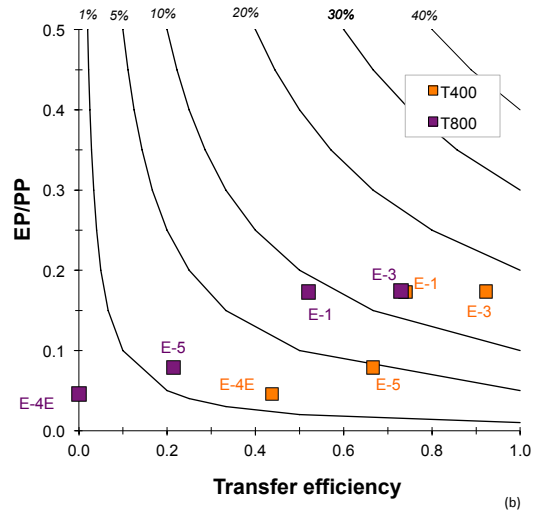
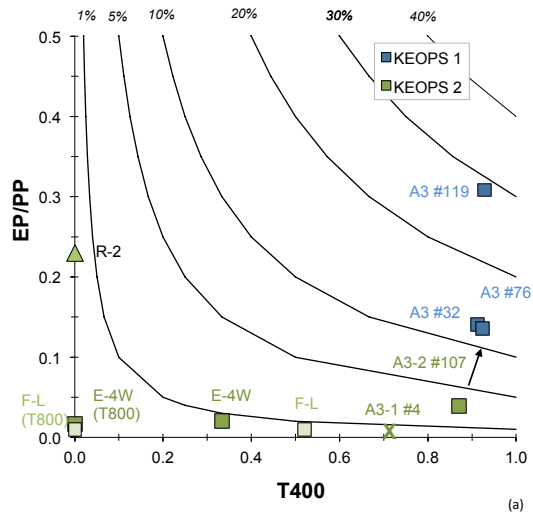
All fluxes in  $\text{mgC m}^{-2} \text{d}^{-1}$

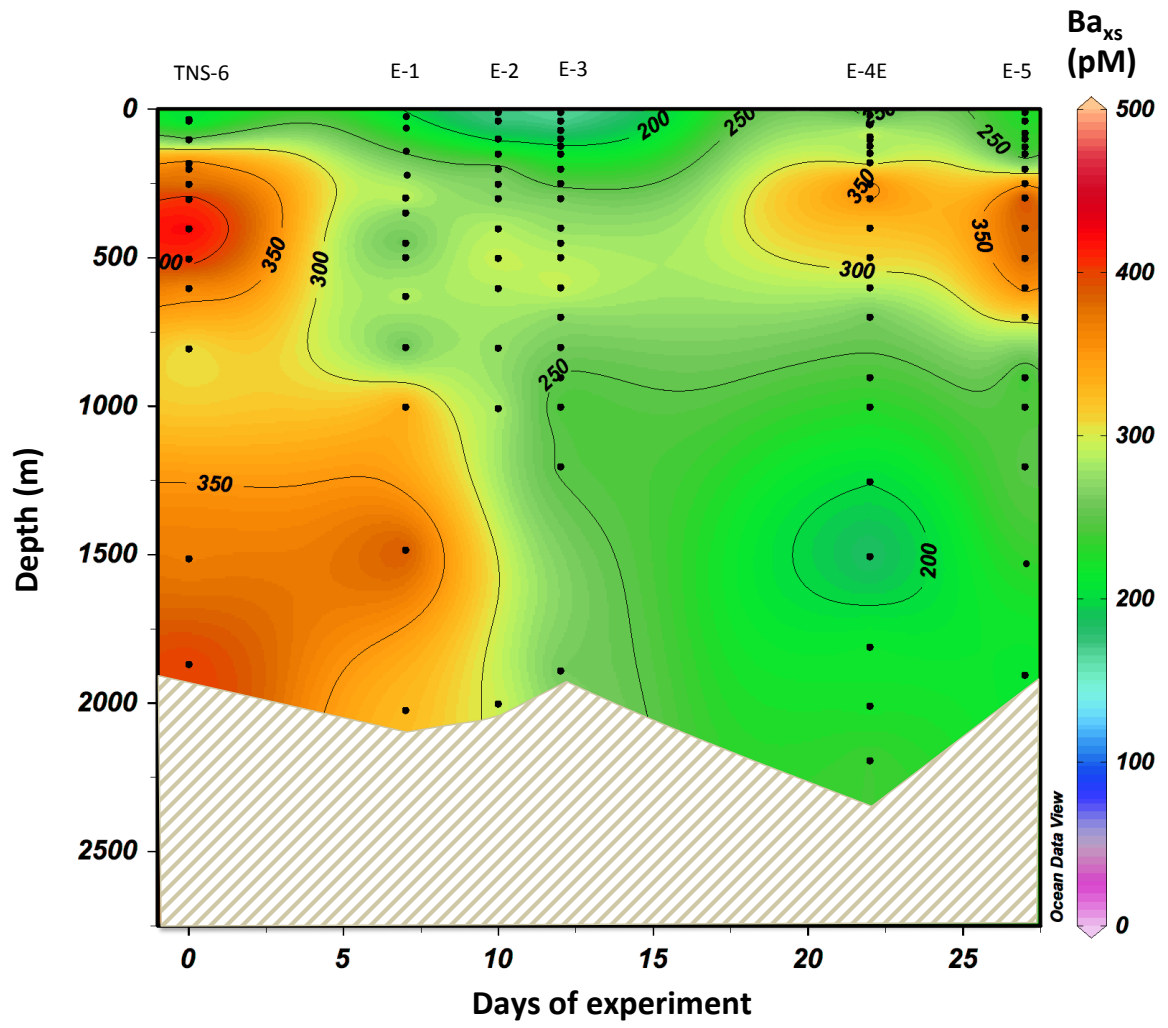
Blue values: r-ratio, mesopelagic remineralization efficiency (MR/EP)

Green values: EP/PP

Red values: MR/PP







Station	CTD cast #	Long (°E)	Lat (°S)	Date of sampling	Seafloor [m]	DWAV <sup>a</sup> Ba <sub>xs</sub> [pM] 150- 400 m	DWAV Ba <sub>xs</sub> [pM] 150- 800 m	MR <sup>o</sup> 150- 400 m [mgC/m <sup>2</sup> /d]	MR Stnd Uncertainty %	MR 150- 800 m [mgC/m <sup>2</sup> /d]	MR Stnd Uncertainty %
<b>Plateau</b>											
A3-1	4*	72.080	50.629	20/10	530	316	/	14	4	/	/
A3-2	107*	72.056	50.624	16/11	527	267	/	11	5	/	/
TEW-3	38	71.018	48.799	31/10	560	324	/	28	8	/	/
<b>Meander time series</b>											
TNS-6	10	72.277	48.779	22/10	1885	427	389	31	7	69	17
E-1	27/30	72.187	48.458	29,30/10	2056	387	325	26	6	48	14
E-2	43	72.077	48.523	1/11	2003	301	309	15	5	42	13
E-3	50/55	71.967	48.702	03,04/11	1915	258	286	10	4	35	12
E-4E	94/97	72.563	48.715	13,14/11	2210	395	357	27	7	58	15
E-5	113/114	71.900	48.412	18/11	1920	402	380	28	7	66	17
<b>Polar Front Zone</b>											
TNS-1	15	71.501	46.833	23/10	2280	350	315	22	6	45	14
TEW-8	47	74.999	48.471	2/11	2786	199	240	2	4	20	11
F-L	63/68	74.659	48.532	06,07/11	2695	345	328	21	6	49	14
<b>Polar Front</b>											
E-4W	81/87	71.425	48.765	11,12/11	1384	468	411	36	8	76	18
<b>Antarctic Zone</b>											
R-2 (Reference site)	17/20	66.717	50.359	25,26/10	2300	572	456	50	10	91	20
TNS-8	8	72.240	49.463	21/10	1030	473	358	37	8	59	15

\*Station A3 (CTD #4 and #107): integration up to 354 and 405 m  
DWAV<sup>a</sup>= Depth weighted average value  
MR<sup>o</sup>= Mesopelagic C remineralization

Station	CTD	MLD [m]	Ez** [m]	PP° Ez [mgC/m <sup>2</sup> /d]	EP°° 150 m [mgC/m <sup>2</sup> /d]	MR 150-400 m [mgC/m <sup>2</sup> /d]	MR 150-800 m [mgC/m <sup>2</sup> /d]	EP/PP	r-ratio 150-400 m	r-ratio 150-800 m	T400	T800
<b>Plateau</b>												
A3-1	4*	161	/	/	47	14	/	/	0.29	/	0.70	/
A3-2	107*	165	38	2172	85	11	/	0.04	0.13	/	0.87	/
<b>Reference site</b>												
R-2	17/20	111	92	132	30	50	91	0.23	1.65	3.02	0	0
<b>Meander time series</b>												
E-1	27/30	84	64	578	100	26	48	0.17	0.26	0.48	0.74	0.52
E-3	50/55	41	68	748	130	10	35	0.17	0.08	0.27	0.92	0.73
E-4E	94/97	77	34	1037	48	27	58	0.05	0.57	1.21	0.43	0.00
E-5	113/114	36	54	1064	84	28	66	0.08	0.33	0.78	0.67	0.22
<b>Polar Front Zone</b>												
F-L	63/68	21	29	3380	43	21	49	0.01	0.48	1.13	0.52	0
<b>Polar Front</b>												
E-4W	81/87	67	31	3287	54	36	76	0.02	0.67	1.41	0.33	0

\*Station A3 (CTD4 and 107); MR integrated up to 354 and 405 m

\*\*EZ euphotic layer (till 1% PAR level)

° PP data from Cavagna et al. (this issue)

°° EP data from PLanchon et al. (this issue)

Station A3

A3-1 CTD4

Table with columns: Niskin, Depth [m], Ba<sub>eq</sub> [pM], Al [nM]. Data rows for CTD4.

A3-2 CTD 107

Table with columns: Niskin, Depth [m], Ba<sub>eq</sub> [pM], Al [nM]. Data rows for CTD 107.

Station RK2

R-2 CTD17

Table with columns: Niskin, Depth [m], Ba<sub>eq</sub> [pM], Al [nM]. Data rows for CTD17.

R-2 CTD 20

Table with columns: Niskin, Depth [m], Ba<sub>eq</sub> [pM], Al [nM]. Data rows for CTD 20.

Station E

E-1 CTD 27

Table with columns: Niskin, Depth [m], Ba<sub>eq</sub> [pM], Al [nM]. Data rows for CTD 27.

E-1 CTD 30

Table with columns: Niskin, Depth [m], Ba<sub>eq</sub> [pM], Al [nM]. Data rows for CTD 30.

E-2 CTD 43

Table with columns: Niskin, Depth [m], Ba<sub>eq</sub> [pM], Al [nM]. Data rows for CTD 43.

E-3 CTD 50

Table with columns: Niskin, Depth [m], Ba<sub>eq</sub> [pM], Al [nM]. Data rows for CTD 50.

Station E (continued)

E-3 CTD 55

Table with columns: Niskin, Depth [m], Ba<sub>eq</sub> [pM], Al [nM]. Data rows for CTD 55.

E-4W CTD 81

Table with columns: Niskin, Depth [m], Ba<sub>eq</sub> [pM], Al [nM]. Data rows for CTD 81.

E-4W CTD 87

Table with columns: Niskin, Depth [m], Ba<sub>eq</sub> [pM], Al [nM]. Data rows for CTD 87.

E-4E CTD 94

Table with columns: Niskin, Depth [m], Ba<sub>eq</sub> [pM], Al [nM]. Data rows for CTD 94.

Station E (continued)

E-4E CTD 97

Table with columns: Niskin, Depth [m], Ba<sub>eq</sub> [pM], Al [nM]. Data rows for CTD 97.

E-5 CTD 113

Table with columns: Niskin, Depth [m], Ba<sub>eq</sub> [pM], Al [nM]. Data rows for CTD 113.

E-5 CTD 114

Table with columns: Niskin, Depth [m], Ba<sub>eq</sub> [pM], Al [nM]. Data rows for CTD 114.

Transect West-East

TEW-3 CTD38

Table with columns: Niskin, Depth [m], Ba<sub>eq</sub> [pM], Al [nM]. Data rows for CTD38.

TEW-8 CTD 47

Table with columns: Niskin, Depth [m], Ba<sub>eq</sub> [pM], Al [nM]. Data rows for CTD 47.

Station F-L

F-L CTD 63

Table with columns: Niskin, Depth [m], Ba<sub>eq</sub> [pM], Al [nM]. Data rows for CTD 63.

F-L CTD 68

Table with columns: Niskin, Depth [m], Ba<sub>eq</sub> [pM], Al [nM]. Data rows for CTD 68.

Transect North-South

TNS-1 CTD15

Table with columns: Niskin, Depth [m], Ba<sub>eq</sub> [pM], Al [nM]. Data rows for CTD15.

TNS-6 CTD 10

Table with columns: Niskin, Depth [m], Ba<sub>eq</sub> [pM], Al [nM]. Data rows for CTD 10.

TNS-8 CTD8

Table with columns: Niskin, Depth [m], Ba<sub>eq</sub> [pM], Al [nM]. Data rows for CTD8.